Optimization of image acquisition parameters in chest tomosynthesis

Experimental studies on pulmonary nodule assessment and perceived image quality

Christina Söderman

Department of Radiation Physics
Institute of Clinical Sciences at
Sahlgrenska Academy
University of Gothenburg

Gothenburg, Sweden, 2016

UNIVERSITY OF
GOTHENBURG

Cover illustration by Merle Horne

Optimization of image acquisition parameters in chest tomosynthesis – Experimental studies on pulmonary nodule assessment and perceived image quality

christina.soderman@gu.se

ISBN 978-91-629-0037-3 (Print)
ISBN 978-91-629-0038-0 (PDF)
http://hdl.handle.net/2077/48658

Printed in Gothenburg, Sweden 2016
INEKO AB

What's this? What's this?
Oh, look
I need to know
What is this?

-Jack Skellington (Danny Elfman)

Abstract

Chest tomosynthesis refers to the technique of acquiring a number of discrete projection images within a limited angular range around the patient. These projection images are then used to reconstruct section images of the chest. Chest tomosynthesis might be a suitable alternative to CT in follow up of pulmonary nodules, which involves nodule size characterization and detection of nodule growth over time. Tomosynthesis section images will contain artifacts due to the limited angular interval of the scan. For example, an in-plane artifact appears as darker areas around nodule borders. There is a need for evaluating the influence of different parameters of a tomosynthesis examination on the resulting section images. The overall aim of this thesis was to find optimal image acquisition parameters in chest tomosynthesis, both in terms of perceived image quality and pulmonary nodule size assessment. In addition, it aims at contributing to a general evaluation of chest tomosynthesis in the task of follow up of nodules, and it includes an evaluation of the effect of the in-plane artifact on nodule size assessment.

Methods including participation of radiologists were used. A visual grading study was performed using an anthropomorphic phantom in order to find the optimal image acquisition parameters regarding perceived image quality. In order to evaluate the quality of the images in terms of nodule measurement accuracy and precision, as well as to evaluate the possibility to detect nodule size change over time, the radiologists measured and visually evaluated the size of simulated pulmonary nodules inserted into clinical chest tomosynthesis images.

With the specific imaging system used, and at the standard dose level, potential benefits for perceived image quality of increasing the dose per projection image do not fully compensate for the negative effects of an accompanying reduction in the number of acquired projection images. Regarding nodule size measurements, the results suggest high measurement accuracy and precision with chest tomosynthesis, and that a reduction of up to 50% of the standard dose level for the imaging system used may be possible without reducing the measurement accuracy and precision. A minor negative effect on nodule measurement accuracy due to the presence of the in-plane artifact was found. Results suggest that chest tomosynthesis is a promising imaging modality for detection of pulmonary nodule growth. However, the possibility to detect growth may decrease with decreasing nodule sizes and dose level. Mismatch in nodule position relative to the reconstructed image planes between two consecutive chest tomosynthesis examinations can also hamper the detection.

In a future perspective, the results presented in this thesis should be confirmed using clinical chest tomosynthesis images including real pulmonary nodules.

Keywords: Chest radiology, chest tomosynthesis, pulmonary nodule, phantoms, hybrid images
ISBN: 978-91-629-0037-3 (Print)
ISBN: 978-91-629-0038-0 (PDF)
E-publication: http://hdl.handle.net/2077/48658

Populärvetenskaplig sammanfattning

I början av 2000-talet introducerades en ny typ av lungröntgenundersökning, lungtomosyntes, till sjukvården. Tekniken innebär att man samlar in ett antal projektionsröntgenbilder av patienten från ett antal olika vinklar, inom ett begränsat vinkelintervall. Projektionsbilderna kan sedan användas för att skapa en typ av snittbilder från vilka man kan få ut mer information om patienten än vad som hade varit möjligt från varje enskild projektionsbild. En lungtomosyntesundersökning kan göras på olika sätt. Till exempel kan man variera vinkelintervallet inom vilket man samlar in projektionsbilder. Man kan också variera antalet projektionsbilder som samlas in inom ett givet vinkelintervall. Energin hos röntgenstrålningen, och den stråldos man använder under undersökningen, kan också varieras. Alla ovan nämnda parametrar påverkar kvaliteten på de slutgiltiga snittbilderna. När det gäller stråldos, så vill man hålla den så låg som möjligt. Detta kan man göra dels genom att minimera stråldosen för varje projektionsbild eller genom ett minska antalet projektionsbilder. Samtidigt vet man att kvaliteten på bilderna sjunker när man minskar stråldosen. I den här avhandlingen presenteras arbete där man sökt efter det sätt att utföra en lungtomosyntesundersökning på som resulterar i bilder med högst kvalitet. Det bästa sättet att utföra en undersökning kan variera beroende på vad man vill använda snittbilderna till. Fokus i den här avhandlingen har varit användandet av lungtomosyntesbilder för att storleksbestämma så kallade lungnoduler, små tumörmisstänkta strukturer i lungorna. Det är viktigt att kunna storleksbestämma noduler med stor noggrannhet eftersom det finns en koppling mellan storlek och risken att de är tumörer. Dessutom är det viktigt med hög precision eftersom det gör det enklare att upptäcka om det skett en storleksförändring av en nodul mellan två undersökningstillfällen. Tillväxt är nämligen också förknippat med högre tumörrisk.

Enligt teorin bör kvaliteten på lungtomosyntesbilderna sjunka när man minskar antalet insamlade snittbilder inom ett givet vinkelintervall eller när man minskar vinkelintervallet. Resultat från den här avhandlingen stämmer bra överens med teorin. Ett bra sätt att genomföra en lungtomosyntesundersökning verkar vara att samla in 60 projektionsbilder inom 30°. Kvaliteten på lungtomosyntesbilder verkar inte påverkas i någon större utsträckning av energin hos röntgenstrålningen.

När det gäller storleksbestämning av noduler tyder resultaten i den här avhandlingen på att man kan mäta nodulers diameter med hög noggrannhet och precision i lungtomosyntesbilder. Dessutom indikerar resultaten att man kan halvera den stråldos som används idag för en lungtomosyntesundersökning utan att påverka kvaliteten på bilderna i sådan mån att noggrannheten för nodulmätningar försämras. Resultaten tyder också på att man med lungtomosyntesbilder kan upptäcka storleksförändringar hos noduler, men att denna möjlighet minskar ju mindre nodulerna är och när man minskar stråldosen.

Arbetet i denna avhandling bygger på simulerade noduler. Nodulerna har lagts in i riktiga patientbilder, vilket gör att resultaten inkluderar vissa effekter av den komplexa anatomiska bakgrunden på mätnoggrannheten, men formen på de simulerade nodulerna är enklare än vad man ser hos riktiga noduler. Fortsatt forskning relaterad till mätnoggrannhet i lungtomosyntebilder och effekten av olika undersökningsparametrar skulle med fördel innefatta riktiga noduler.

List of papers

This thesis is based on the following papers, referred to in the text by their Roman numerals.

I. Söderman, C., Asplund, S., Allansdotter Johnsson, Å., Vikgren, J., Rossi Norrlund, R., Molnar, D., Svalkvist, A., Månsson, L.G., Båth, M. *Image quality dependency on system configuration and tube voltage in chest tomosynthesis – A visual grading study using an anthropomorphic chest phantom*. Medical Physics 2015 Mar;42(3):1200-1212. http://dx.doi.org/10.1118/1.4907963

II. Söderman, C., Allansdotter Johnsson, Å., Vikgren, J., Rossi Norrlund, R., Molnar, D., Svalkvist, A., Månsson, L.G., Båth, M. *Evaluation of accuracy and precision of manual size measurements in chest tomosynthesis using simulated pulmonary nodules.* Academic Radiology 2015 Apr;22(4):496-504. http://dx.doi.org/10.1016/j.acra.2014.11.012

III. Söderman C., Allansdotter Johnsson Å., Vikgren J., Rossi Norrlund R., Molnar D., Svalkvist A., Månsson L.G., Båth M. *Effect of radiation dose level on accuracy and precision of manual size measurements in chest tomosynthesis evaluated using simulated pulmonary nodules.* Radiation Protection Dosimetry 2016 Jun;169(1-4):199-203. http://dx.doi.org/10.1093/rpd/ncw041

IV. Söderman C., Allansdotter Johnsson Å., Vikgren J., Rossi Norrlund R., Molnar D., Svalkvist A., Månsson L.G., Båth M. *Influence of the in-plane artefact in chest tomosynthesis on pulmonary nodule size measurements.* Radiation Protection Dosimetry 2016 Jun;169(1-4):188-198. http://dx.doi.org/10.1093/rpd/ncv536

V. Söderman C., Allansdotter Johnsson Å., Vikgren J., Rossi Norrlund R., Molnar D., Mirzai, M., Svalkvist A., Månsson L.G., Båth M. *Detection of pulmonary growth with chest tomosynthesis: a human observer study using simulated nodules and simulated dose reduction.* Submitted

Related presentations of preliminary results

Söderman, C., Allansdotter Johnsson, Å., Vikgren, J., Rossi Norrlund, R., Molnar, D., Svalkvist, A., Månsson, L.G., Båth *Accuracy of pulmonary nodule size measurement on chest tomosynthesis*. Swedish Medical Physics Conference (Nationellt möte om sjukhusfysik), November 13 – 14, 2013, Varberg, Sweden

Söderman, C., Asplund, S., Allansdotter Johnsson, Å., Vikgren, J., Rossi Norrlund, R., Molnar, D., Svalkvist, A., Månsson, L.G., Båth, M. *Påverkan av systemkonfiguration och rörspänning på bildkvaliteten i lungtomosyntes – en visual grading-studie med antropomorft lungfantom.* Swedish Medical Physics Conference (Nationellt möte om sjukhusfysik), November 13 – 14, 2014, Varberg, Sweden

Söderman, C., Allansdotter Johnsson, Å., Vikgren, J., Rossi Norrlund, R., Molnar, D., Svalkvist, A., Månsson, L.G., Båth, M. *Diameter measurement accuracy of simulated pulmonary nodules on chest tomosynthesis images.* 3rd Annual SWE-RAYS Workshop, August 20 – 22, 2014, Malmö, Sweden

Söderman C., Allansdotter Johnsson Å., Vikgren J., Rossi Norrlund R., Molnar D., Svalkvist A., Månsson L.G., Båth M. *Effect of radiation dose on pulmonary nodule size measurements in chest tomosynthesis.* Optimisation in X-ray and Molecular Imaging – Fourth Malmö Conference on Medical Imaging, May 28 – 30, 2015, Gothenburg, Sweden

Söderman C., Allansdotter Johnsson Å., Vikgren J., Rossi Norrlund R., Molnar D., Svalkvist A., Månsson L.G., Båth M. *Influence of the in-plane artefact in chest tomosynthesis on pulmonary nodule size measurements.* Optimisation in X-ray and Molecular Imaging – Fourth Malmö Conference on Medical Imaging, May 28 – 30, 2015, Gothenburg, Sweden

Söderman, C., Allansdotter Johnsson, Å., Vikgren, J., Rossi Norrlund, R., Molnar, D., Mirzai, M., Svalkvist, A., Månsson, L.G., Båth, M. *Detection of pulmonary nodule growth with dose reduced chest tomosynthesis: a human observer study using simulated nodules.* SPIE Medical Imaging 2016: Image Perception, Observer Performance, and Technology Assessment, February 27 – March 3, 2016, San Diego, USA

Content

Abbreviations

ANOVA	Analysis of variance
AUC	Area under the curve
AUC_{ROC}	Area under the ROC curve
AUC_{VGC}	Area under the VGC curve
CT	Computed tomography
CXR	Conventional chest radiography
DICOM	Digital Imaging and Communications in Medicine
DQE	Detective quantum efficiency
FPF	False positive fraction
ICS	Image criteria score
LAT	Lateral
MITS	Matrix inversion tomosynthesis
MRMC	Multiple-reader multiple-case
MTF	Modulation transfer function
NPS	Noise power spectrum
PA	Posteroanterior
ROC	Receiver operating characteristics
ROI	Region of interest
SAA	Shift-and-add
SID	Source-to-image distance
TPF	True positive fraction
VDT	Volume doubling time
VGA	Visual grading analysis
VGC	Visual grading characteristics
VGR	Visual grading regression
ViewDEX	Viewer for Digital Evaluation of X-ray images

1. Introduction

In thoracic radiology, conventional chest radiography (CXR) is the most common examination performed [1]. The technique offers a quick overview of the general cardiopulmonary status of the patient and is associated with high accessibility, relatively low effective doses (0.05 – 0.1 mSv for a combined posteroanterior (PA) and lateral (LAT) view) as well as low financial cost [2-7]. Being a 2D projection imaging technique, CXR has however been shown to be limited by low sensitivity in terms of subtle lung pathology, due to it being potentially obscured in the image by overlaying anatomy [8-15]. With the use of computed tomography (CT), this problem is solved by the 3D visualization of the patient in tomographic slices in which the overlaying anatomy is removed. Although new CT technology and reconstruction algorithms have led to possibilities of reducing the resulting radiation dose to the patient from a CT examination [16], most clinical tasks still result in effective doses up to several mSv [7, 17-20], considerably higher than that for a CXR examination. Additionally, the examination time and cost are higher than CXR.

In the early 2000s, tomosynthesis was introduced as an interesting alternative in thoracic radiology [21-26]. A chest tomosynthesis examination is performed with modified conventional radiography equipment that allows the X-ray tube to move along a certain path relative to the detector while low dose projection images are acquired within a limited angular range. These projection images are then used to reconstruct section images of the chest. The resulting section images contain much less of the overlaying anatomy than the projection images, providing some resolution in the depth direction. Reported dose levels from a chest tomosynthesis examination are in the range of 0.1 – 0.2 mSv [3-7, 20, 27-29].

The impact of this possibility of achieving increased diagnostic information as compared to CXR, without a considerable increase in dose, is yet not fully estimated. Specifically, the optimal utilization of tomosynthesis in the clinical practice of thoracic radiology, in relation to CXR and CT, has not been established. Initial investigations concerning the role of chest tomosynthesis in clinical practice have mainly been focused on its use as a problem-solving modality for verifying unresolved lesions detected on CXR [29-32].

Furthermore, the scientific evaluation of chest tomosynthesis has been focused on detection and follow-up of pulmonary nodules. These are rounded structures, less than 3 cm in diameter, localized in the lung parenchyma and can be indicators of a malignant disease. In comparison to CXR, clinical studies have shown a threefold increase in the sensitivity of pulmonary nodule detection with chest tomosynthesis [5, 7, 18, 20, 27, 33]. Figure 1 shows examples of a CXR image, a chest tomosynthesis image and a coronal CT image from a patient presenting with a pulmonary nodule, illustrating the increased visibility with tomosynthesis as compared to CXR.

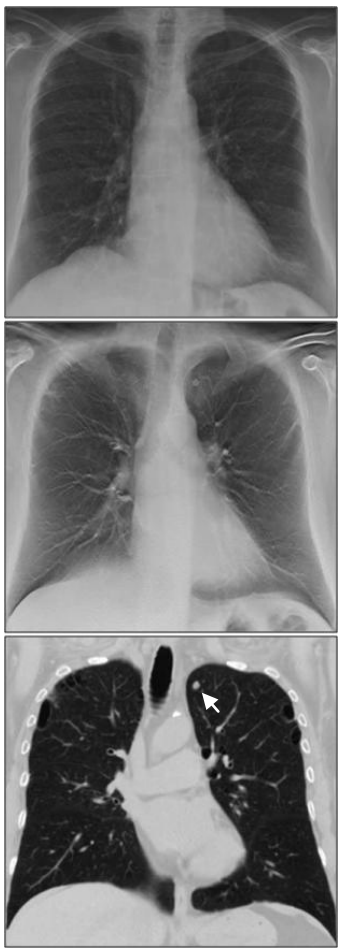

Figure 1*: A CXR image (top), a coronal chest tomosynthesis image and a coronal CT image (bottom) from the same patient. A nodule (position pointed out in the CT image) is present in the upper left lung lobe.*

Since growth of pulmonary nodules is an important indicator of malignancy, a detected pulmonary nodule is often followed up by repeated CT scans as a means of detecting or ruling out any size changes of the nodule. It has been suggested that chest tomosynthesis might be a suitable alternative for CT in the follow up of pulmonary nodules [24]. The task of pulmonary nodule follow up involves size measurements of nodules. In order for an imaging technique to be used for this task, it is of importance to make sure that the measurement accuracy and precision are on a clinically acceptable level so that size changes of clinical relevance can be detected with acceptable sensitivity. In addition, management strategies for detected nodules are stratified according to nodule size [34, 35]. Thereby, high measurement accuracy is of importance for nodule characterization. The limited angular range of the tomosynthesis scan leads to an incomplete sampling of the frequency space. One effect of this is the presence of an in-plane artifact appearing as darker areas above and below structures, in the direction of the tomosynthesis scan [36, 37]. The artifact will often appear around nodules (Figure 2), possibly hampering the accuracy of nodule size measurements.

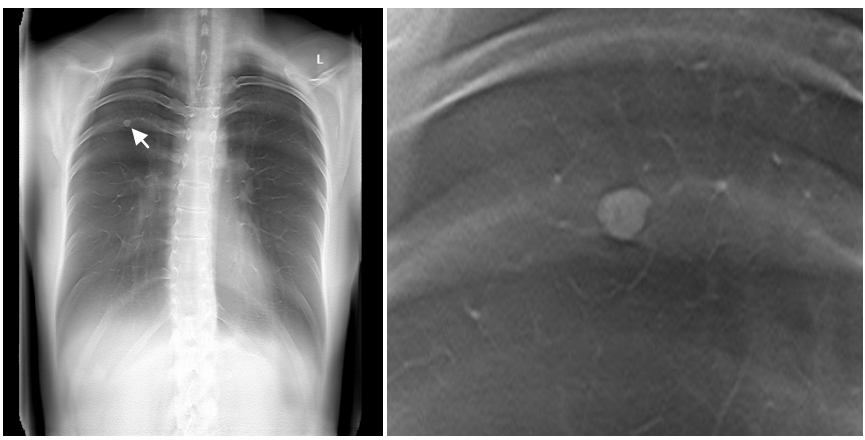

***Figure 2**: A chest tomosynthesis section image from a patient with a 9 mm pulmonary nodule. An in-plane artifact, inherent to the tomosynthesis technique, is apparent as darker areas around the nodule. The artifact can also be seen along the borders of the ribs visible in the image. The tomosynthesis scan resulting in the section image was performed in the craniocaudal direction.*

As chest tomosynthesis is a relatively new technique, there is a need for evaluating how different parameters for the tomosynthesis examination will influence the resulting section images. Image acquisition parameters such as angular range covered by the acquired projection images, number of acquired projection images, and the dose level used for each projection image can all be expected to influence the image quality. Finding the optimal setting, both in terms of perceived image quality and for the clinical task of pulmonary nodule follow up, is of importance.

2. Aims

The overall aim of this thesis was to find optimal settings for image acquisition parameters in chest tomosynthesis, both in terms of perceived image quality and pulmonary nodule size assessment. In addition, it aims at contributing to a general evaluation of the clinical usefulness of chest tomosynthesis in the task of follow up of detected pulmonary nodules. The specific aims of the papers included in the thesis were

- to find the optimal settings for dose per projection image, angular range covered of the projection images, number of projection image acquired and tube voltage in terms of perceived image quality in chest tomosynthesis (Paper I),

- to assess the accuracy and precision of diameter measurements of pulmonary nodules in chest tomosynthesis images, and how these two measures depend on nodule size and radiation dose level (Papers II and III),

- to investigate the effect of the in-plane artifact, visible around pulmonary nodules, on the accuracy and precision of diameter measurements on pulmonary nodules (Paper IV) , and

- to investigate the feasibility of detecting pulmonary nodule growth with chest tomosynthesis and its dependency on dose level, nodule size and position of the nodule relative to the plane of focus (Paper V).

3. Background

3.1 Tomosynthesis

Tomosynthesis X-ray imaging refers to the technique of acquiring a discrete number of low-dose 2D projection images within a limited angular range around the patient, and using these projection images to reconstruct section images in which structures at certain depths in the patient are brought into focus [21, 23]. The principle of the technique is similar to that of conventional geometric tomography, in which a continuous exposure is used while the X-ray tube and imaging detector move in opposite directions. However, whereas tomography only generates one plane of focus per scan, one tomosynthesis scan results in an arbitrary number of focus planes. In tomosynthesis, a plane of focus is achieved by shifting the acquired projection images relative to each other and adding them together. Multiple planes of focus throughout the patient can be generated by shifting the projection images with varying amounts. See Figure 3 for an illustration of the technique. Tomosynthesis has mainly been applied to breast imaging, orthopedic imaging, and chest imaging, the latter being the focus of the work in this thesis.

Theoretical descriptions of the idea of both conventional tomography and tomosynthesis were first presented in the 1930s [38]. Observed limitations of the 2D radiography technique in imaging 3D anatomy prompted the development of techniques for depth localization. Conventional tomography was shortly after its introduction adopted in the medical imaging community, but practical issues hindered the development of tomosynthesis. The idea of rapid acquisition of multiple discrete low dose radiographs would require large area detectors with fast read out and high detective quantum efficiency (DQE), i.e. a detector with high X-ray detection efficiency. No such detectors existed at the time. Additionally, the image reconstruction technique for tomosynthesis would demand computational power that was not at hand at the time. It was not until the introduction of flat panel detectors in the beginning of the 2000s that all the technical prerequisites enabling tomosynthesis were available and the interest for the technique increased.

With the shift-and-add (SAA) reconstruction technique shortly described above, structures outside the plane of focus will be superimposed over the image and appear blurred. Various techniques for reducing this blurring and thus increasing the contrast of objects in the plane of focus exist [21]. The most common is to apply filters in the frequency domain to the projection radiographs before the shift-and-add is performed; similar to filtered backprojection in CT. Due to the limited angular range of the tomosynthesis scan, no complete removal of overlaying structures in the tomosynthesis images can be achieved. The appearance of out of plane-structures will depend on for example the angular range of the tomosynthesis scan and the number of projection images acquired. Machida et al. [39] review this dependency in more detail. At a certain threshold distance from an out-of-plane structure, the blurring of the structure in the tomosynthesis image of the plane of focus will change into ripple, potentially hampering the clinical image quality of the images. For a given angular range of the tomosynthesis scan, the minimum distance from a structure at which ripple will occur in the image plane will increase with increasing number of acquired projection images. In the case of chest tomosynthesis, the ribs are a prominent source of out-of-plane blur or ripple. Figure 3 illustrates the occurrence of out-of-plane blur or ripple in the images. The angular range used for the tomosynthesis scan will in turn affect the depth resolution, such that the larger the angular range the higher the depth resolution. Optimizing parameters for the acquisition of the projection images in tomosynthesis involves finding an acceptable level of the residuals of out-of-plane structures. Additionally, as in all X-ray imaging modalities, optimization of tomosynthesis imaging also includes finding the dose level corresponding to acceptable quantum noise in the final images. As mentioned in the Introduction, the limited angular range of the tomosynthesis scan also leads to an in-plane artifact appearing as darker areas above and below structures, in the direction of the tomosynthesis scan (Figure 2) [36, 37].

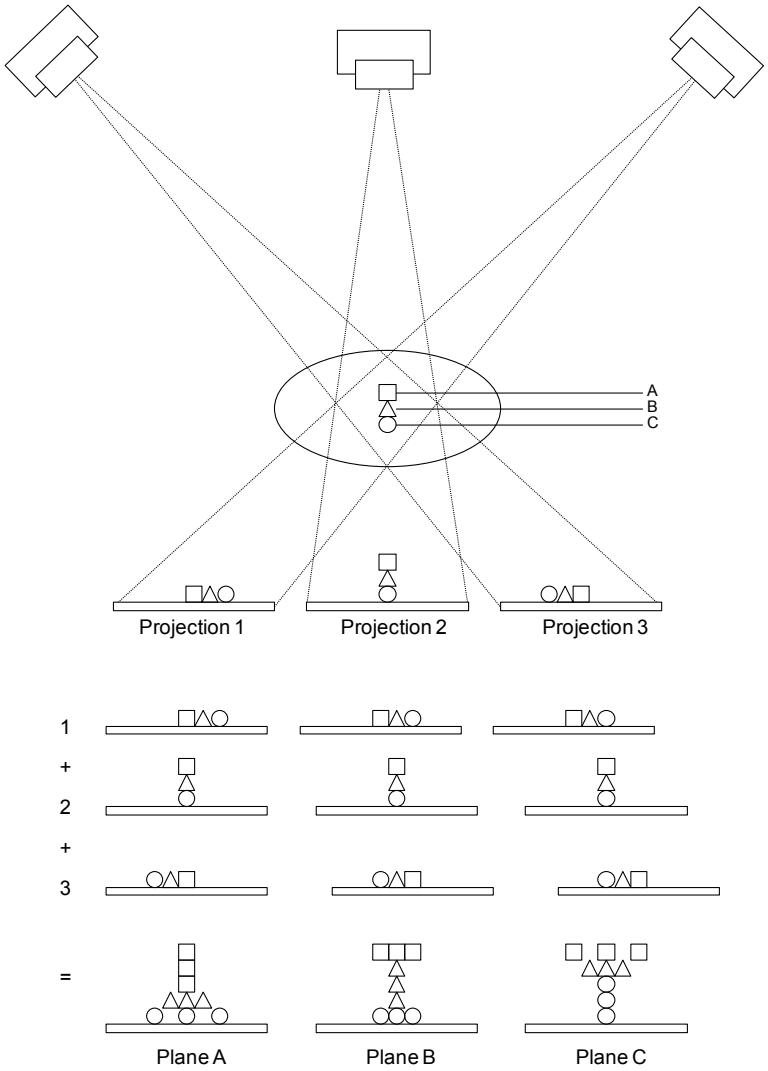

***Figure 3**: Illustration of the shift-and-add technique used for reconstruction of tomosynthesis images, and of the appearance of out-of-plane structures in the final section images. In this example, three discrete projection images are acquired at three different angles. Structures at plane A, B and C in the imaged object are projected at different locations in the projection images. The projection images are shifted relative to each other and added to bring structures at a certain depth into focus. Which plane in the imaged object that is brought into focus depends on the amount of shift applied to the projection images. In the example in the figure, the image with plane A in focus will include out-of-plane blur from structures located in plane B, while structures located in plane C will instead appear as ripple. The image with plane B in focus will contain out-of-plane blur from plane A and C. In the image of plane C in focus, structures located in Plane B will be sufficiently blurred, but structures in Plane A will appear as ripple.*

3.1.1 Chest tomosynthesis

Currently there are three manufacturers supplying commercially available systems for chest tomosynthesis imaging: Fujifilm (Tokyo, Japan), Shimadzu (Kyoto, Japan), and GE Healthcare (Chalfont St Giles, UK). The systems are modified conventional chest radiography system or systems initially intended for fluoroscopy. They consist of an X-ray tube, a flat-panel detector and an anti-scatter grid [24, 26]. In order to perform the tomosynthesis scan, the system allows the X-ray tube to perform a sweeping linear motion relative to detector during exposure, while keeping the X-ray tube facing the center of the detector throughout the sweep. The patient is most commonly positioned in a similar manner as is the case for a conventional upright PA-view CXR examination. Figure 4 shows a schematic description of a chest tomosynthesis imaging system. A chest tomosynthesis scan takes approximately 5 – 10 seconds depending on the system used. This requires patients to hold their breath in order to avoid respiratory motion to hamper the final image quality.

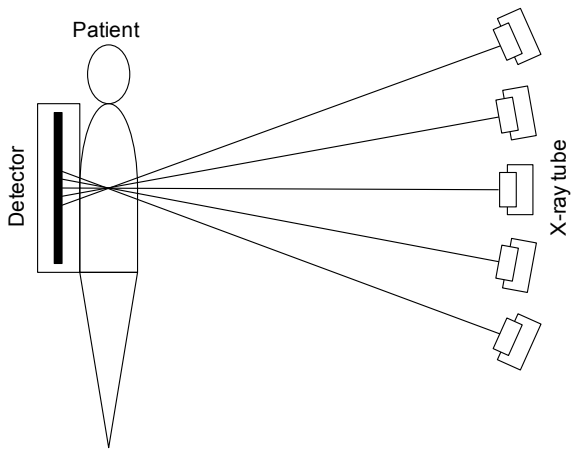

***Figure 4**: A schematic description of a chest tomosynthesis imaging system.*

A summary of clinical evaluations of chest tomosynthesis is given in Section 3.3. Several of these studies have been focused on detection and management of pulmonary nodules, including Papers II – V in this thesis. Therefore, Section 3.2 gives a short overview of pulmonary nodules and their impact on thoracic radiology.

3.2 Pulmonary nodules

A pulmonary nodule is defined as a structure confined within the lung parenchyma and that appears as a rounded or irregular radiographic opacity with a diameter of less than 3 cm [40]. Pulmonary nodules may represent neoplasms, infections and congenital abnormalities. Neoplasms can be either benign or malignant. A malignant nodule can be either an early stage of lung cancer or a metastasis from a primary cancer somewhere else in the body [41]. Available data concerning the prevalence of pulmonary nodules are mainly from studies investigating lung cancer screening using low dose chest CT. A review of such studies by Wahidi et al. [42] revealed that one or more nodules were detected in 8 – 51% of included patients. The reported variation in prevalence can partly be attributed to differences in CT slice thickness used in the studies, as well as to differences in the proportion of smokers included in the study populations [42]. Pulmonary nodules are also frequent incidental findings in CXR or chest CT examinations performed due to other clinical issues. Hall et al. [43] investigated the prevalence of incidental findings on chest CT angiograms ordered to assess pulmonary embolism. They found pulmonary nodules in 22% of the included 589 patients.

According to the British Thoracic Society, nodules can be divided into two main categories in terms of density: solid and sub-solid nodules [35]. The sub-solid nodules are either of pure ground glass opacity, defined as a slight increase in density as compared to surrounding anatomy but through which the underlying vascular structures can be seen, or contain both a solid and ground-glass component.

In the majority of cases, nodules have a benign cause. Wahidi et al. [42] found that the prevalence of malignancy among nodules detected in lung cancer screening studies was 1.1 – 12%. Nevertheless, lung cancer has a high mortality rate and a pulmonary nodule might be an early stage of lung cancer. The National Lung Screening Trial, conducted in the U.S., has shown that early diagnosis of lung cancer reduces the mortality from lung cancer [44], making the management of these lesions an important issue in the thoracic radiology community.

3.2.1 Management of pulmonary nodules

One important factor when differentiating between malignant and benign nodules is the size of the nodule at detection. The NELSON trial, investigating the use of low dose CT in lung cancer screening, found that the probability of developing lung cancer for participants with nodules with a volume less than 100 mm^3 or a maximum diameter less than 5 mm did not significantly differ from that of participants with no detected nodules [45]. Intermediate risk of lung cancer was found for participants with nodules with a volume of 100 – 300 mm^3 or a diameter of 5 – 10 mm, while a high risk was found for nodules larger than that. Another important indicator of malignancy for pulmonary nodules is growth and growth rate. Growth rate of pulmonary nodules are often given in volume doubling time (VDT), i.e. the time it takes for the nodule to double in volume. In the NELSON trial [45], VDTs were determined based on volume or diameter measurements of nodules on two consecutive CT scans and by assuming an exponential growth. It was found that nodules with VDT of 600 days or more did not indicate a significant increase in lung cancer probability. A low risk for lung cancer was found for nodules with VDTs of 400 – 600 days while a high risk was found for nodules with VDTs of less than 400.

In accordance with the results described above, proposed management strategies concerning the differentiation of nodules as benign or malignant commonly depend on the size of the nodule at detection [34, 35]. Recommendations state that detected small nodules (< 5 mm) not predictive of lung cancer should not be further evaluated. Larger nodules (>10 mm) should be referred for diagnostic work up, for example with positron emission tomography-CT or needle biopsy tests. Recommendations for intermediate sized nodules, however (~ 5 – 10 mm), include follow up of the nodule with repeated chest CT scans at certain time intervals. In this way, possible growth of the nodule might be detected. If the nodule shows clinically relevant growth, further diagnostic work up should be initiated. The sizes of pulmonary nodules are usually assessed by either using manual diameter measurements or volumetric segmentation [35].

3.3 Clinical evaluations of chest tomosynthesis

3.3.1 Sensitivity compared to CXR

The expected improvement in sensitivity of chest tomosynthesis compared to CXR has been confirmed in previous studies for various findings related to pulmonary disease, such as mycobacterial disease [17], cystic fibrosis [46], aortic arch calcification [47], pulmonary emphysema [6], asbestosis and pleural plaques [48], and airway lesions [49]. Several authors have compared the detection rate of pulmonary nodules of chest tomosynthesis and CXR, using nodules detected at CT as a reference [5, 7, 18, 20, 27, 33]. These studies show unanimous results in terms of relative performance of the two imaging modalities, indicating a roughly threefold increase in sensitivity in terms of pulmonary nodule detection with chest tomosynthesis as compared to CXR. However, the absolute performance for each modality differs between the studies. For example, in a study by Vikgren et al. [33], 56% of all included nodules were detected with chest tomosynthesis and 16% were detected with CXR, while corresponding detection rates in a study by Yamada et al. [5] were 80% and 37%, respectively. This difference in absolute detection rates could be due to the fact that the study material in the study by Yamada et al. included a smaller proportion (50%) of small nodules (≤ 6 mm) than the study by Vikgren et al. (64%). In another study, by Dobbins et al. [7], 79% of the nodules were smaller than or equal to 6 mm and the detection rate was 13.5% for tomosynthesis and 3.8% for CXR. The differences in detection rate can also be explained by variations in decision thresholds when judging a nodule as present in the patient or not. Additionally, the specialties of the radiologists included in that study varied over a wide range and only one of them had any clinical experience of chest tomosynthesis. Regarding the specificity, in the study by Vikgren et al., tomosynthesis resulted in 50% more false positive findings than CXR. Dobbins et al. on the other hand, demonstrated no significant difference in false positive rate between the two modalities. All above-mentioned studies showed an increase in detection rate with nodule size.

Hwang et al. [28] and Asplund et al. [50] investigated the effect of dose level on pulmonary nodule detection in chest tomosynthesis. Hwang et al. scanned a chest phantom including artificial nodules at two dose levels corresponding to 0.14 mSv and 0.062 mSv. The study could not show any significant difference in nodule detection between the two dose levels for nodules ranging in size from 4 mm to 8 mm. In the study by Asplund et al. clinical chest tomosynthesis images

were used together with a method for simulating a dose reduction of the images. Nodules detected at CT for the included patients were used as a reference. The study could not demonstrate a significant difference in pulmonary nodule detection between images corresponding to an effective dose of 0.12 mSv and 0.04 mSv.

Some limitations regarding nodule detection in chest tomosynthesis have been pointed out in previous studies. For example, Asplund et al. [51] have listed a number of potential pitfalls regarding nodule detection in chest tomosynthesis images. One of the identified difficulties concerned pulmonary nodules located close to the pleural border. Due to the limited angular range of the tomosynthesis scan, which in turn leads to limited depth resolution in the reconstructed images, these nodules might be misinterpreted as pleural or subpleural changes. Studies have also shown that chest tomosynthesis might be limited in the detection of low-density ground glass nodules [5, 52].

3.3.2 Chest tomosynthesis in the clinical practice

In conjunction to the introduction of chest tomosynthesis as an interesting alternative in thoracic X-ray imaging, Dobbins and McAdams [24] proposed four scenarios for the integration of chest tomosynthesis in the clinical practice:

1. As a complement to or replacement of CXR examinations for some patients.

2. As a complement to or replacement of CXR examinations for all patients.

3. As a modality for evaluation of suspicious lesions found on CXR.

4. As a modality for follow up of known pulmonary nodules.

A number of studies have evaluated the use of chest tomosynthesis as a problem-solving modality, as proposed in scenario 3 above. The clinical challenge addressed in this scenario regards lesions detected on CXR that cannot with a certain level of confidence be confirmed as being located within the lung or not, nor be ruled out as composite normal anatomical structures, a so called pseudolesion. To verify the nature of the lesion, the patient is in many cases referred to a CT examination. However, as CT is a limited resource in many clinics, this could lead to a delay in the diagnosis for these patients. In the scenario proposed by Dobbins and McAdams [24], a chest tomosynthesis examination would be performed in direct conjunction with the CXR

examination on the same X-ray equipment. If the chest tomosynthesis examination cannot confirm or rule out a lesion, or if it indeed can confirm a lesion that requires further work up, the patient can be sent to CT with higher priority. For cases where chest tomosynthesis can rule out the presence of a lesion, unnecessary CT scans are avoided. Quaia et al. have evaluated to what extent chest tomosynthesis obviated the need for CT in cases with uncertain findings on CXR [29-32]. With general inclusion criteria for patients, they found that chest tomosynthesis resolved 75% of doubtful CXR cases [31, 32]. For patients with a known malignancy, chest tomosynthesis resolved 50% of cases [29]. In a study by Johnsson et al. [53], all chest tomosynthesis examinations performed in the clinical routine during one month at one institution were reviewed. The study showed that 80% of the CT scans that were judged to have been performed instead of chest tomosynthesis had chest tomosynthesis not been an option were obviated by the use of chest tomosynthesis. From the same institution, Petersson et al. [54] retrospectively evaluated CXR, chest tomosynthesis and CT cases and found that, by using criteria based on scientific evidence and clinical experience, chest tomosynthesis has the potential to substitute 20% of CXR examinations and 25% of CT examinations performed at a thoracic radiology department.

In scenario 4 above, chest tomosynthesis would replace CT, which is currently the standard modality for the clinical task of follow up of pulmonary nodules. Studies have supported the use of chest tomosynthesis for follow up of known pulmonary nodules. In terms of visibility of known pulmonary nodules, Lee et al. [55] found that 50% of nodules found with computer-aided detection in CT images were also visible in chest tomosynthesis. However, the majority of the non-visible nodules (93%) were smaller than 5 mm and accordingly not indicative for follow up as recently suggested. Dobbins et al. [56] also investigated the visibility of nodules in chest tomosynthesis and found that 70% of nodules 5 – 10 mm detected on CT were visible in retrospect on chest tomosynthesis images. Using chest tomosynthesis for nodule follow up requires that the technique is sufficiently accurate regarding assessing the size of the nodule, so that an appropriate management strategy is chosen, and in detecting size change. Johnsson et al. [57] performed a phantom study where the diameters of spheres with known sizes in a homogenous background were measured both in tomosynthesis images and in CT images. The measurement error was comparable between the two modalities. In another study by Johnsson et al. [58], radiologists measured the diameter of real clinical nodules found in patients in tomosynthesis and CT images. Exact knowledge of the true sizes of the nodules was not available, but segmented diameters from the CT images were used as

reference. No systematic bias between diameters measurements in the two modalities was found and the measurement repeatability was similar.

Papers II – V in this thesis aim to contribute to the scientific evaluation of chest tomosynthesis for use in follow up of pulmonary nodules.

3.4 Image quality evaluation

In the work presented in this thesis, the quality of chest tomosynthesis images has been evaluated by using methods that included participation of experienced thoracic radiologists. In Paper I, a visual grading study was performed in order to find the optimal image acquisition parameters in terms of perceived image quality. In Papers II – V, thoracic radiologists measured the size of artificial pulmonary nodules inserted into clinical chest tomosynthesis images in order to evaluate the quality of the images in terms of measurement accuracy and precision. In Papers I, III and V, a method for simulating a dose reduction of the images was also used. Paper V evaluated the possibility to detect nodule size change over time and included the use of receiver operating characteristic (ROC) analysis. The following four subsections (3.4.1 – 3.4.4) discuss the use of clinical images with added artificial pathology or noise, so called hybrid images, in evaluation of image quality; describes the use of ROC analysis and visual grading in evaluation of medical images; and reviews different approaches for evaluating the quality of medical images in terms of pulmonary nodule measurements. See Chapters 4 and 5 for a detailed description of the specific study designs and image material used in Papers I – V.

3.4.1 Hybrid images

The fundamental task of the radiologist in the clinical practice is to detect pathology in radiological images. This task will be limited partly by the quantum noise present in the images. However, in clinical radiology, and in particular for projection imaging and for tomographic imaging techniques where no complete removal of overlapping anatomy in the images is achieved, it is foremost the anatomical background in the images that sets the limit for sensitivity [8-15]. It can be anticipated that the anatomical background will also affect the accuracy of observers in measuring nodule size, due to for example difficulties in delineating the borders of nodules in the images. Consequently, in studies

evaluating radiological images, the highest clinical validity is obtained when clinical patient images are used. It can however be cumbersome to collect patient images with an appropriate distribution of pathology for the particular study. One way to get around this is to use anthropomorphic phantoms, mimicking as closely as possible anatomical backgrounds found in patients and containing artificial pathology. Another possibility is to add simulated pathology to clinical patient images. The latter types of images are an example of hybrid images. By using hybrid images in this way, it is possible to control the characteristics of the pathology in terms of, for example, size, localization, and attenuation. Various methods for inserting simulated pulmonary nodules in clinical images have been used in studies concerning detection sensitivity in CXR and chest CT images [8-14, 59-61]. Depending on the imaging system used, the required complexity of the simulated structures of the nodule will differ. The method used in this thesis for simulating the presence of pulmonary nodules in chest tomosynthesis images has been presented previously by Svalkvist et al. [62, 63] and Svensson et al. [64]. See Section 4.2 for a description of this method.

An important aspect of radiographic imaging is to optimize the radiation dose level used. This kind of optimization work includes assessing the effect of dose level on the quality of the images. Following the reasoning above concerning the importance of including anatomical background in the evaluation of radiological images, this would require repeated exposures of patients. For ethical reasons, this is not always achievable. Anthropomorphic phantoms could of course be used in this case as well, but a more sophisticated method would be to use hybrid images consisting of clinical images to which noise corresponding to a certain dose level has been added. In this way, it is possible to simulate that the images have been acquired with a lower radiation dose than what was actually the case. Methods, with varying levels of complexity, for adding noise to radiographic images in order to simulate a dose reduction of the image have been presented [65-69]. In its simplest form, simulation of dose reduction of an image is performed by adding white noise to the image. This is done by adding a random number, derived from a Gaussian distribution with a mean of zero and a standard deviation depending on the pixel value, to each pixel. Using this method will result in an image with the same standard deviation in pixel values as an image actually acquired at the wanted lower dose level, but the frequency distribution of the noise, given by the noise power spectrum (NPS), will differ [68]. Other methods, which take the frequency distribution of the noise into account and thereby increase the validity of the dose reduction, have been suggested [65-67, 69]. For example, Båth et al. [66] proposed a method for simulating a dose reduction in conventional radiography images that resulted in images with

similar NPS as images actually acquired at the lower dose. This is done by adding a noise image to the original image. Knowledge of the NPS at two dose levels close to the original dose level and the simulated lower dose level is used to determine the NPS of the noise image. The method is based on the assumption that the DQE of the imaging system is constant between the dose level closest to the simulated lower dose level at which the NPS is known and the simulated lower dose level, as well as between the dose level closest to the original dose level at which the NPS is known and the original dose level. Additionally, the DQE is assumed to be constant within the dose range existing in one image. In the case of tomosynthesis projection images, which are acquired at relatively low doses, the above-mentioned assumptions about the DQE in the method proposed by Båth et al. might be violated as the DQE of digital detectors drop quickly with dose at low dose levels. Therefore, Svalkvist and Båth [69] further developed the previous method so that variations in DQE at relevant dose ranges are taken into account, thereby increasing the validity of the method of dose reduction when applied to chest tomosynthesis images. The adapted method by Svalkvist and Båth was used in Papers I, III and V and is described in more detail in Section 4.3.

3.4.2 Receiver operating characteristics analysis

The previous subsection mentioned the detection of pathology in radiological images as the fundamental task of the radiologist. A more accurate description of the task is that it involves determining if the images are from a healthy patient or a diseased patient. One way of evaluating the quality of radiological images is to quantify the possibility of observers to perform the differentiation of healthy and diseased patients using the images. As measures of this possibility, sensitivity and specificity can be used. Sensitivity is the probability that a diseased patient is actually judged as being diseased by the radiologist, and specificity is the probability that a healthy patient is actually judged as being healthy by the radiologist. For a given observer, the resulting sensitivity and specificity will depend on the decision threshold of the observer. A correlation between sensitivity and specificity exists, such that an increase in sensitivity, due to a shift in the decision threshold of the observer, will lead to an accompanying decrease in specificity. Consequently, comparing different observers using these measures can be difficult (See Subsection 3.3.1 regarding the comparison of nodule detection rates between different studies).

With ROC analysis, a measure that is independent of the decision threshold of the observers can be determined [70, 71]. This is done by letting observers use a multi-step rating scale, ranging from being certain that the image is from a healthy patient to being certain that the image is from a diseased patient, instead of just presenting it as a binary task (healthy or diseased). In this way, a sampling of the observers' decisions at different thresholds can be performed. The rating data is used to establish the trade-off between the true positive fraction (TPF), which is equal to the sensitivity, and the false positive fraction (FPF), which is defined as 1-specificity. The TPF is plotted against the FPF for each decision threshold and a curve, referred to as an ROC curve, is fitted to the data. Different models for the underlying distributions of the rating data for the healthy and diseased patients can be used for the fitting of the curve. For example, a binormal model, assuming two Gaussian distributions, can be used. Another possibility is to perform a trapezoidal fit by adjoining the data points with straight lines. Regardless of the model used for fitting the curve, the final measure of the possibility of the observers to distinguish between healthy and diseased patients using the images is given by the area under the obtained ROC curve (AUC_{ROC}). The AUC_{ROC} can take values between 0.5 and 1. An AUC_{ROC} of 0.5, achieved when the curve coincides with the diagonal, indicates a chance-level performance of the observers while an AUC_{ROC} of 1 indicates perfect differentiation between healthy and diseased patients. Figure 5 illustrates rating data distributions and a corresponding curve from an ROC study.

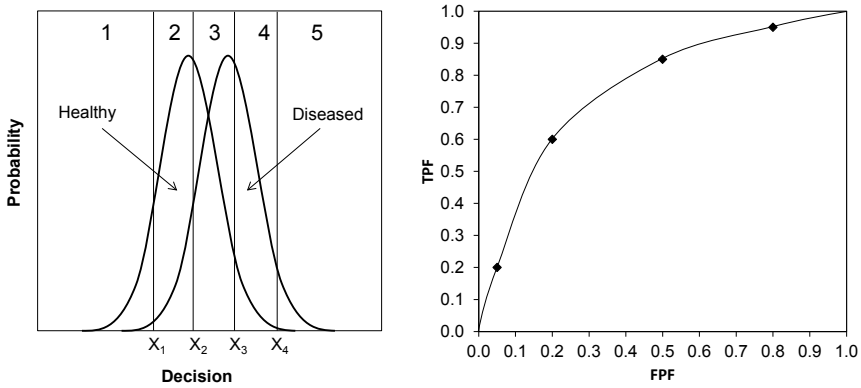

Figure 5: *Left: Probability distributions of rating data for healthy and diseased patients from an ROC study including a five-step rating scale. A five-step rating scale corresponds to four decision thresholds. Right: The resulting ROC curve, given by the TPF as a function of FPF.*

3.4.3 Visual grading

In visual grading studies concerning medical images, observers rate the visibility of certain anatomical structures in the images [70, 72]. The use of this method for image quality evaluation is based on the assumption that the possibility to detect pathology is correlated to the reproduction of anatomical structures. It can be used for comparing different acquisition settings within one imaging modality, or for comparing different modalities. Different approaches and study designs of visual grading exist. For example, determined image quality criteria concerning anatomical structures and their required level of reproduction can be used. By letting observers judge if each criterion is fulfilled or not, an image criteria score (ICS) given by the proportion of the fulfilled criteria can be determined for each tested condition or modality. Another approach, referred to as visual grading analysis (VGA), is to identify a number of relevant structures and let the observers judge the visibility of the structures on a numerical multi-step scale. This can be done either as a relative comparison with a reference image or in terms of absolute visibility. The result of a VGA study is a VGA score, which is determined by averaging the ratings over all observers and all cases in each tested condition or modality. The averaging can be performed over each structure as well, depending on whether there is an interest in determining the VGA score separately for each structure or not. This is also the case for the ICS.

One important disadvantage of the VGA score is that the calculation of an average value from the numerical rating data is not allowed statistically. This is a consequence of the numerical values in the rating scale being in fact ordinal data, i.e. they have a natural ordering, but it is not necessarily the case that the difference between the different steps are equivalent. Regarding this issue, two analysis methods that handle visual grading data as ordinal data have been presented, namely visual grading regression (VGR) [73-76] and visual grading characteristics (VGC) [77-79].

In VGR, the rating data is analyzed using ordinal logistic regression, appropriate for the case of ordinal dependent variables [73-76]. This statistical method is designed to handle multiple factors affecting the studied outcome variable, and is thus valuable in studies where the effect of several conditions on image quality is studied simultaneously. For example, the effect of imaging equipment as well as image post-processing could be evaluated in one study. Additionally, the use of VGR makes it possible to control for potentially confounding factors such as observer and patient identity.

With VGC analysis, rating data from a multi-step scale regarding the fulfillment of image quality criteria is used to produce a VGC curve [77-79]. This is done by plotting the proportion of ratings above a certain threshold for a tested imaging condition against the same proportion for another condition, serving as reference, as the threshold is varied. As such, the procedure is similar to that of the handling of data in an ROC analysis. As a figure of merit, representing the difference between the two tested conditions in terms of separation between the two rating distributions, the area under the resulting VGC curve (AUC_{VGC}) is used. An $AUC_{VGC} = 0.5$ indicates no overall difference between the two tested conditions. An $AUC_{VGC} < 0.5$ indicates a generally better image quality of the reference condition while an $AUC_{VGC} > 0.5$ indicates that the alternative condition results in the best image quality. Software that allows for statistically correct determination of the uncertainty of the result of the VGC data has been developed [78, 79]. This software was used in Papers I and V and is described in more detail in Section 4.4.

Regarding suitable image quality criteria to use in a visual grading study, the European commission has established such criteria for a range of conventional radiography and CT examinations, including CXR [80] and chest CT [81]. Quality criteria to be used in the case of chest tomosynthesis have been proposed by Asplund et al. [51]. The proposed criteria are mainly based on the European criteria for CT. An adaption was made so that structures relevant for tomosynthesis were included. A modified version of the set of criteria proposed by Asplund et al. was used in Paper I. These are listed in Table 2 in Chapter 5.

Visual grading studies can be performed with either clinical images from patients or using images of an anthropomorphic phantom. The use of a phantom is advantageous when ethical considerations hinder the use of clinical images. When using phantom images in a visual grading study, it is of importance to make sure that the phantom includes relevant anatomical structures and that the resemblance to real anatomy is on an acceptable level. Nevertheless, one should keep in mind that the results of a visual grading study based on images of only one phantom will not include the effect of the natural variation in anatomy found among patients.

3.4.4 Studies of nodule size measurements in medical images

Recent studies evaluating size measurement of pulmonary nodules in radiological imaging have mainly been focused on CT images, since this currently is the gold-standard modality for pulmonary nodule follow up. The designs of presented studies vary regarding included image material. For example, simple non-anatomical phantoms containing spheres mimicking nodules [82, 83] or anatomical phantoms containing artificial nodules [84-88] have been used. Hybrid images, consisting of clinical images to which artificial nodules or noise have been added have, also been used [89-91]. Many studies are however based on real clinical nodules found in patients [92-101].

The main advantage of using phantoms with artificial nodules is that the ground truth regarding pulmonary nodule size is known, which allows for determination of any absolute bias in the measurements [82, 83, 85]. Phantoms have been used in controlled experiments in order to predict the effect of different imaging parameters in CT, such as image slice thickness and dose level, on the clinical measurement error [86, 88]. Results in terms of magnitude of absolute measurement accuracy from these studies should however be interpreted as a lower bound for what is achievable in clinical cases as these will include more complex backgrounds and nodules with more irregular borders. The use of hybrid images allows for taking the effect of more complex anatomical backgrounds into account. At the same time, the size of the nodules can be controlled. Funaki et al. [90] used simulated nodules inserted into clinical images in order to study the accuracy of software for volumetric measurements of nodules. Sun et al. [89] used a similar study design to assess a method for detecting pulmonary nodule size change.

Studies including real clinical nodules have been used to evaluate the effect of different imaging parameters, such as exposure level or reconstruction technique, on nodule size measurements as well as intraobserver and interobserver variability [91, 93, 94, 96, 98, 99]. A common method for evaluating the ability to detect nodule growth in CT images is to scan patients twice within a few minutes or to evaluate nodules that have been proven to be stable in size over a substantial time period [92, 95, 97, 102]. In this manner, a follow up situation where no growth of the nodule has occurred is achieved. By analyzing the variability in subsequent measurements of the nodules, a limit in nodule growth detection using the images can be estimated. This method of analyzing nodules showing no growth is often chosen since it is difficult to establish ground truth concerning the amount with which growing nodules have increased in size. It does however not include the ability of the radiologist to, in addition to the

measurement results, take perceived proximity and size of the nodule relative to other anatomical structures such as vessels and bronchi in the image plane into account and might therefore underestimate the possibility of detecting nodule growth in the clinical situation [103].

4. Material and methods

In this chapter, a summary of the material and methods used in Papers I – V is given.

4.1 Chest tomosynthesis system

All clinical images and phantom images used in the work presented in this thesis were acquired with the GE Definium 8000 radiographic system with the VolumeRAD tomosynthesis option (GE Healthcare, Chalfont St Giles, UK). This system is provided with a cesium iodide flat panel detector with 2022 × 2022 pixels and a pixel size of 0.2 mm × 0.2 mm. The default configuration for a chest tomosynthesis examination includes the acquisition of 60 projection images distributed evenly over an angular range of 30° around the standard orthogonal PA direction. The X-ray output is constant for all projection images and is determined by the resulting exposure of a scout radiograph. This scout is a conventional PA projection acquired prior to the tomosynthesis scan with automatic exposure control at a source-to-image distance of 180 cm. The tube load used for the scout is multiplied by a user-adjustable dose ratio and distributed evenly between the 60 tomosynthesis projection images. In the work presented in this thesis, the dose-ratio was set to 10. Possible tube load settings for the tomosynthesis projection images follow the Renard scale and the resulting tube load per projection image is rounded down to the closest value on this scale. The minimum possible tube load is 0.25 mAs. The default tube voltage used for the acquisition of the scout and the tomosynthesis scan is 120 kV and a total filtration of 3 mm Al + 0.1 mm Cu is used. During the acquisition of the tomosynthesis projection images, the X-ray tube performs a continuous vertical motion while rotating around its own axis so that the central beam of the X-ray field passes through the same point during the entire angular sweep. This pivot point is located 9.9 cm above the detector surface, towards the X-ray tube. The system automatically adjusts the collimation during the scan in order to compensate for the increase in field size at the detector surface for the oblique acquisition angles. For a standard-sized patient (170 cm and 70 kg), the effective dose resulting from a chest tomosynthesis examination, with this system, using

the default settings, has been determined to 0.12 mSv [4], not including the scout.

The GE system performs a cone-beam filtered backprojection with an incorporated 3D view-weighting technique for the reconstruction of the section images [104]. With this algorithm, non-uniformity artifacts due to that the entirety of the imaged volume will not be covered by all acquired projection images, in turn due to the limited angular range of the tomosynthesis scan, are suppressed. This is done by adjusting the intensity of each voxel according to the number of times the X-ray beam passes through that voxel during the scan. The system allows the user to define the volume for which images are to be reconstructed, as well as the interval between each section image. Possible intervals are given in steps of 1 mm, with the smallest being 1 mm. In the work presented in this thesis, an interval of 5 mm between the reconstructed images was used.

4.2 Simulation of pulmonary nodules

In Papers II – V, a method previously described by Svalkvist et al. [62, 63, 105] and Svensson et al. [57] for simulating the presence of pulmonary nodules in chest tomosynthesis images was used. With this method, 3D artificial nodules are created and inserted into the raw-data projection images prior to the reconstruction of tomosynthesis images. The computer code used for the generation of the nodules and for the insertion in the projection images is written in IDL 6.3 (RSI, Boulder, CO, USA). The simulated nodules are virtually placed in 3D space at locations corresponding to desired positions within the lung parenchyma of the patient. By using knowledge of the acquisition geometry of the chest tomosynthesis system, the paths of the X-rays from the focal spot to the detector are traced and the amount of attenuation of the radiation in the nodule is calculated. For each of the acquired projection images, the resulting signal reduction in the detector due to the presence of the nodule can thereby be sampled and stored in a template as floating point values between 0 and 1. Signal blurring in the detector is then taken into account by applying the modulation transfer function (MTF) of the tomosynthesis system to the pixels in the template. The nodule template is thereby somewhat larger than the projected size of the nodule in order to allow for a broadening of the nodule profile. The signal strength is adjusted according to expected contrast loss due to scattered radiation. This adjustment is based on previous results from Monte Carlo simulations by Ullman et al. [106]. Additionally, effect of patient motion on the

nodule signal is simulated by applying a randomized shift in the position of the nodule between each insertion in the projection images. The nodule is finally inserted in the images by multiplying the pixel values in each raw-data projection image with the values stored in the corresponding nodule template.

Figure 6 shows examples of simulated nodules used in Papers II-V. In Papers II – IV, the above-described method was used to insert spheroid-shaped nodules in clinical chest tomosynthesis images. In Paper V, nodules with more realistic appearances, approximately spherical in shape with smooth irregularities and a rough surface structure, as originally proposed by Svalkvist et al. [62, 63, 105], were used. The proposal is based on morphological descriptions in previous studies and on evaluations of appearances of nodules in CT and tomosynthesis images at the authors' department. These simulated nodules are created by first creating a sphere with a given radius. Smaller spheres, with radii randomized between 10% and 50% of the radius of the original sphere, are then added to the original sphere at randomized positions relative to the center of the original sphere. This will introduce the wanted irregularities in the nodule shape. A rough surface structure is obtained by additionally adding a large number of smaller spheres with radii randomized between 1% and 10% of the original sphere. Three-dimensional mean filters are applied to the nodule array after the addition of the smaller spheres in order to smooth the shape. The border of the final nodule is determined by assigning a value of 1 to all voxels with a value of 0.5 or above whereas voxels with a value below this threshold is assigned a value of 0. Different appearances of created nodules are obtained partly by the randomization of the position of the additional smaller nodules, but also by randomizing the number of smaller nodules and their sizes. All inserted nodules are assumed to be of homogenous density with an attenuation coefficient defined by the user.

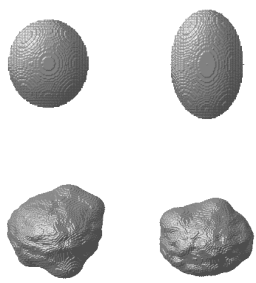

Figure 6*: Examples of simulated nodules used in the work presented in this thesis. The spheroid-shaped nodules in the top panel were used in Papers II, III and IV. The nodules in the bottom panel, with more clinically realistic appearances, were used in Paper V.*

Regarding the similarity of the simulated nodules with realistic appearance to real nodules found in patients, Svalkvist et al. performed a study to compare the visual appearance and detection rate of the simulated nodules to that of real nodules [63]. An observer performance study was conducted with radiologists as observers. Their task was firstly to detect nodules, and rate their confidence of detection, in an image material containing both simulated and real nodules. After this, the observers were presented with the image material again, this time with the location of the nodules pointed out to them. The instruction to the observers was to rate their confidence that the nodule was real or not. A modified ROC analysis was used to test the significance of the difference between the rating data for the simulated nodules and the real nodules. The study could not show any difference in detection between real and simulated nodules. However, to a limited extent, the observers were able to separate the simulated nodules from real nodules in terms of visual appearance.

In conjunction with the preparation for the work presented in this thesis, an artifact affecting the appearance in the section images of simulated nodules located in low signal regions of the tomosynthesis projection images was discovered. Svensson et al. have recently described the artifact and the cause of it in detail [64]. The artifact manifested as a blurred nodule border resulting in that the nodules appeared larger than what was actually the case. After a review of the computer code used for the implementation of the simulation method, it was concluded that the reason for the artifact was a function that rounded floating-point values resulting from multiplication of a floating-point value and an integer down to the closest integer. As the application of MTF is performed in the frequency domain, all pixel values in the nodule template are affected by the filtering process. Consequently, all values stored in the nodule template will be smaller than 1. When the template is multiplied with the integer values in the image matrix, the above-mentioned rounding function will result in that all pixel values multiplied with the nodule template will be reduced by at least a value of 1. Even image pixels corresponding to pixels in the nodule template close to the edge of the template, which should not be affected, will be reduced in value. The relative change in pixel values in the image matrix will depend on the original pixel values in the region where the simulated nodule is inserted, such that the lower the pixel values, the larger the relative effect and, accordingly, the more visible the artifact will be. As described by Svensson et al., the computer code has been rewritten so that floating-point numbers are rounded to the closest integer number. Thereby the effect on the image pixels of the filtering process of the nodule template will be minimized.

In Papers II, IV and V, the corrected version of the method was used. The measurements in Paper III were however performed before the effect of the unknown rounding function was discovered. After a review of an experienced thoracic radiologist where nodules inserted with the corrected code were compared with nodules inserted with the uncorrected code in terms of apparent size and visibility, it was however judged that the effect of the undesired rounding function was negligible for nodules located in high signal regions of the images. The study was therefore deemed valid for nodules with positions corresponding to this criterion.

After the study presented in Paper III was conducted, the corrected version of the code was used by Svensson et al. [64] in a study replicating the work by Svalkvist et al. [63] for comparing the detection rate and appearance of the simulated nodules and real nodules. Svensson et al. found that the corrected code resulted in an increase in similarity to real nodules concerning visual appearance as compared to the uncorrected code. However, it was found that the detection rate was higher for the simulated nodules. As mentioned, nodules in high-signal regions of the images are not affected by the artifact caused by the undesired rounding function. Based on this, Svensson et al. made two conclusions regarding the results of the study. Firstly, that the reason for the observed higher detection rate with the corrected code was that the detection rate for nodules in low-signal regions of the images increased when the induced artifact was removed. Secondly, that the detection rate for the nodules in the high-signal regions of the images was probably slightly too high, as compared to real nodules, for both the corrected and uncorrected version of the code. In the study by Svalkvist et al., where the uncorrected code was used, the resulting average detection rate of the nodules in low-signal regions and high-signal regions was similar to that of real nodules. The reason for the increase in detection with the corrected code was assumed to be that the inherent in-plane artifact visible around nodules, mentioned in the Introduction, became more apparent. This in-plane artifact has been suggested to improve detection of lesions in breast tomosynthesis [37]. Implications of this finding in the study by Svensson et al. on the work presented in this thesis are discussed in Chapter 6.

4.3 Simulation of dose reduction

In Papers I, III and V a method previously described by Svalkvist and Båth [69, 105] for simulating a dose reduction of chest tomosynthesis examinations was used. As described in Subsection 3.4.1, the method is an adapted version of an

earlier method described for use in conventional radiography at dose levels where the variation in DQE is assumed to be small. In the case of chest tomosynthesis, the low dose used for the acquisition of the projection images is at a level where the electronic noise is non-negligible and therefore the DQE of the imaging system may show a dependency on the dose [69]. This is accounted for in the adapted method used in the work presented in this thesis.

Firstly, the method requires that sets of flat-field images, containing only noise, be acquired at different dose levels with the tomosynthesis imaging system. From the flat-field images, the relationship between pixel value and variance is determined for each angle of the tomosynthesis projections. Additionally, the NPS is determined for all acquired flat-field images. The pixel values in each projection image acquired during the chest tomosynthesis examination for which the dose reduction is to be applied are scaled down according to the desired lower dose level. Mean pixel values in relevant regions in the original projection image and the scaled version of each original projection image are then determined. For each projection image, the two flat-field images, matched with the projection images according to angle of projection, that closest match the mean pixel value of the original projection image and the scaled version of the original projection image are then identified. A noise image is created in the spatial domain by assigning normally distributed, floating point, pseudorandom numbers with a mean of zero and standard deviation of one to the pixels. The noise image is Fourier transformed and a filter consisting of frequency components determined by using the NPS of the two selected flat-field images is applied. Possible differences in DQE between the dose level of the original projection image and the dose level of the flat field image closest matching the original projection image in dose, as well as between the dose level of the scaled version of the original projection image and the flat-field image closest matching the scaled version of the original projection image in dose, will lead to a loss of proportionality between dose and pixel variance between these two dose ranges. This is corrected for in the creation of the noise image by using the established relationship between pixel values and pixel variance in the determination of the applied frequency filter. The frequency filter is given by the square root of the NPS of the noise image, which is given by Equation 1.

$$NPS(u, v)_{Im_{noise}} = \left(\frac{\sigma_{D_{sim}}}{\sigma_{D_1}}\right)^2 NPS(u,v)_{D_1} - \left(\frac{D_{sim}}{D_{orig}}\right)^2 \left(\frac{\sigma_{D_{orig}}}{\sigma_{D_2}}\right)^2 NPS(u,v)_{D_2} \quad (1)$$

In Equation 1, D_1 and D_2 refers to the dose levels at which the flat-field images that, in terms of mean pixel value, closest match the scaled version of the original projection image and the original version of the projection image were

acquired, D_{sim} refers to the desired lower dose level and D_{orig} refers to the dose level at which the original projection image was acquired. $NPS(u, v)_{Im_{noise}}$ is the NPS of the noise image, $NPS(u,v)_{D_1}$ and $NPS(u,v)_{D_2}$ are the NPS of the flat-field images acquired at D_1 and D_2, and σ is the standard deviation of pixel values at dose levels D_1, D_2, D_{sim} and D_{orig}. The standard deviations are determined using the established relationship between pixel values and variance using the flat-field images.

After the filtering of the noise image, it is inversely Fourier transformed and a correction for differences in DQE between the dose levels that exist within the image at the original and the simulated dose levels is then applied to the pixel values in the noise image according to Equation 2.

$$Im(x,y)_{noise,\,corr} = Im(x,y)_{noise,\,uncorr} \sqrt{\frac{\sigma^2_{D_{Im(x,y)_{sim}}} - \sigma^2_{D_{Im(x,y)_{orig}}} \left(\frac{D_{sim}}{D_{orig}}\right)^2}{\sigma^2_{D_{sim}} - \sigma^2_{D_{orig}} \left(\frac{D_{sim}}{D_{orig}}\right)^2}} \quad (2)$$

In Equation 2, $Im(x,y)_{noise,\,corr}$ is the corrected noise image, $Im(x,y)_{noise,\,uncorr}$ is the original uncorrected noise image, $D_{Im(x,y)_{sim}}$ is the dose level at a given location in the scaled version of the original projection image and $D_{Im(x,y)_{orig}}$ is the dose level at a given location in the original projection image. Finally, the noise image is added to the scaled version of the original projection image. Svalkvist and Båth [69] showed that the method results in reconstructed chest tomosynthesis images with similar NPS as what an examination actually acquired at the lower dose level would result in.

4.5 VGC analysis software

In Papers I and V, VGC Analyzer [78, 79], a software tool designed for performing VGC analysis, was used. VGC Analyzer can handle rating data from fully crossed multiple-reader multiple-case (MRMC) studies, i.e. studies including multiple observers and multiple cases and in which all the observers assess all the cases. It determines the AUC_{VGC} averaged over all observers. The asymmetric 95% confidence interval of the AUC_{VGC} is determined using a resampling technique referred to as bootstrapping. A null hypothesis that the two tested conditions are equal (H_0: $AUC_{VGC} = 0.5$) is assumed and tested. The p-value is determined by using a permutation resampling technique. Correlated

data between the two tested conditions are taken into account in the resampling techniques used for the uncertainty calculation and the testing of the null hypothesis. VGC Analyzer performs the analysis both for the fixed-reader situation and for the random-reader situation. With a fixed-reader analysis, the results are only applicable to the actual observers in the study, while the results in a random-reader analysis are applicable to the population of observers. Results based on both a binormal and a trapezoidal fit of the VGC curve are given by the software. Although originally designed for performing VGC analysis, VGC Analyzer can also handle rating data from MRMC ROC studies and determine accompanying ROC curves.

4.6 Display of images

In all papers included in this thesis, a software tool dedicated for use in observer performance studies including medical images was used. The software – ViewDEX (Viewer for Digital Evaluation of X-ray images) [107-109] – is compatible with the Digital Imaging and Communications in Medicine (DICOM) file format and allows the observer to both view the images and provide responses to any included tasks. Medical grade DICOM-calibrated monitors were used to display the images.

For all papers, the included images were presented to the each radiologist in a unique random order. The radiologists were free to alter the window width and level as well as to use the magnification function in ViewDEX. In Papers II – V, investigating nodule size and growth assessment, images were displayed with a certain degree of magnification and a built-in tool for performing 2D measurements in the images was used by the radiologists. Figure 7 shows an example of the use of this measurement tool.

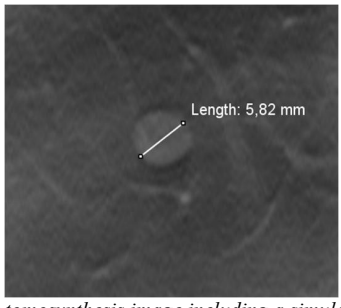

Figure 7*: Cutout from a chest tomosynthesis image including a simulated nodule. A measurement of the nodule has been performed with the tool provided by ViewDEX. The result of the measurement is presented as an overlay in the image.*

5. Summary of papers

In this chapter, an overview of the design and results of the studies presented in Papers I – V is given. See Chapter 6 for a more detailed discussion of the obtained results.

Paper I: Image quality dependency on system configuration and tube voltage in chest tomosynthesis – A visual grading study using an anthropomorphic chest phantom

As mentioned in Section 4.3, the dose used for the acquisition of chest tomosynthesis projection images is at such a level that the detector is operated at a signal level where the DQE may show a dependency on the dose [69]. Increasing the dose per projection image could of course improve the DQE and thereby reduce the noise in the final reconstructed images. In order to keep the total dose to the patient unaltered, this would require that the total number of projection images be decreased. This can be done by either reducing the projection image density, defined as the total number of projection images acquired divided by the angular range within which they were acquired, or by reducing the angular range of the tomosynthesis scan. However, the image acquisition configuration will, as discussed in Section 3.1, affect the appearance of out-of-plane structures in the reconstructed tomosynthesis images. The optimal configuration will thus be a compromise between the number of projection images acquired, the angular range covered by the projection images and the dose per projection image.

The most common tube voltage for chest tomosynthesis is 120 kV, which is also common for CXR examinations. This relatively high tube voltage is used in CXR in order to suppress the appearance of the ribs in the images. Since the overlaying anatomy is, to a large extent, removed in chest tomosynthesis images, another tube voltage might be optimal.

In Paper I, the aim was to investigate the potential benefit in terms of image quality of increasing the dose per projection image in chest tomosynthesis by reducing the angular range of the tomosynthesis scan or by reducing the

projection image density. Additionally, the aim was to evaluate the influence of tube voltage on the image quality.

A visual grading study in which four thoracic radiologists participated as observers was performed. The image material consisted of 90 coronal tomosynthesis image series of an anthropomorphic chest phantom (PBU-X-21, Kyoto, Kagaku Co. Ltd., Kyoto, Japan). The images were acquired with the GE VolumeRAD tomosynthesis system. Nine different combinations of projection image density and angular ranges, as listed in Table 1, were represented with the image series.

***Table 1**: Tomosynthesis image acquisition configurations included in Paper I.*

	Number of projection images (n)	Angular range (°)	Projection image density (n/°)
Default	60	30	2
1	40	30	1.33
2	30	30	1
3	20	30	0.67
4	15	30	0.5
5	40	20	2
6	30	15	2
7	20	10	2
8	15	7.5	2

Each image acquisition configuration was acquired with ten different tube voltages, ranging from 60 kV to 150 kV in steps of 10 kV. All included image series represented acquisitions that would result in the same effective dose to a patient. As the possibility of freely choosing configurations during the tomosynthesis scan with the VolumeRAD system was restricted, the default configuration was used for all the evaluated configurations. In the reconstruction of the images, only the projection images corresponding to the evaluated configurations were used. By combining a manipulation of the filtration used for the scout images with a simulated dose reduction, using the method described in Section 4.3, the projection images could be acquired in such a way that the different configurations corresponded to equal total effective dose.

In Table 2, the image quality criteria used in the study are listed. The observers individually rated the image series according to how well they fulfilled each criterion. A five level rating scale was used.

***Table 2**: Image quality criteria used in the visual grading study performed in Paper I.*

1	Clear reproduction of the trachea
2	Clear reproduction of the large and medium sized vessels
3	Possibility to follow vessels through the volume
4	Clear reproduction of the small sized vessels as seen 1 cm from the costopleural border, Anterior
5	Clear reproduction of the small sized vessels as seen 1 cm from the costopleural border, Central
6	Clear reproduction of the small sized vessels as seen 1 cm from the costopleural border, Posterior
7	Reproduction of the paratracheal tissue
8	Reproduction of the thoracic aorta
9	Clinically acceptable artifacts

VGC analysis of the rating data was performed using VGC Analyzer using a fixed-reader analysis. The analysis was performed in terms of image acquisition configuration and tube voltage, using the default configuration and 120 kVp, respectively, as reference. For the assessment of image acquisition configuration, rating data were combined for all tube voltages. For the assessment of tube voltage, rating data were combined for all image acquisition configurations.

Figure 8 presents the AUC_{VGC} for each combination of image acquisition configuration and image quality criterion. Concerning the angular range, a tendency of increasing image quality with decreasing angular range was seen for the criteria related to the reproduction of the trachea and paratracheal tissue. Additionally, for the criteria related to the reproduction of large and medium sized vessels and the thoracic aorta, the results indicated an improved image quality for configurations with smaller angular range than the default configuration. However, a decreased angular range of the tomosynthesis scan negatively affected the possibility to follow vessels through the volume. For all image quality criteria, except that related to the reproduction of the thoracic aorta, a tendency of decreasing image quality with decreasing projection image density was seen. In Figure 9, examples of images resulting from the default configuration, the configuration including 15 projection images covering 30°, and the configuration including 15 projection images covering 7.5° are shown. Figure 10 presents the AUC_{VGC} for each tube voltage and image quality criterion. In general, the image quality showed little dependency on the tube voltage.

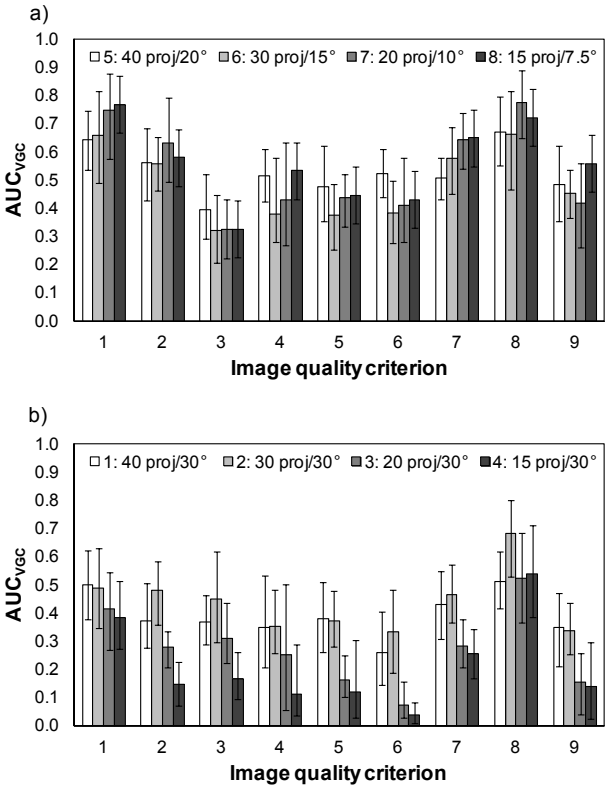

***Figure 8**: AUC_{VGC} for tomosynthesis configurations with **a)** varying angular interval and **b)** varying projection image density. Error bars represent the 95% confidence interval. See Table 2 for a description of the image quality criteria.*

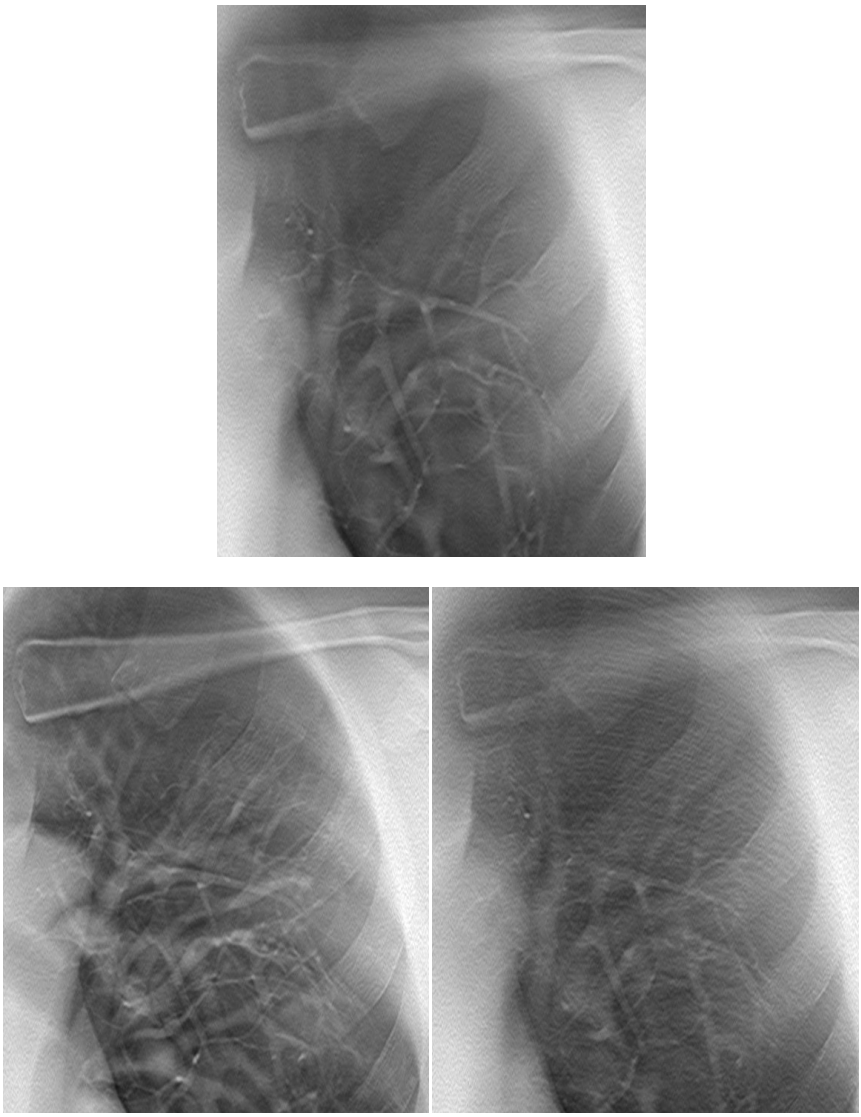

Figure 9*: Cutouts from tomosynthesis section images included in Paper I. The upper image is the result of the default configuration (60 projection images covering 30°). The image at the bottom left is the results of a configuration including 15 projection images covering 7.5°. The image at the bottom right is the result of a configuration including 15 projection images covering 30°. A ripple-artifact resulting from insufficient blurring of the posterior ribs is visible in the bottom right image.*

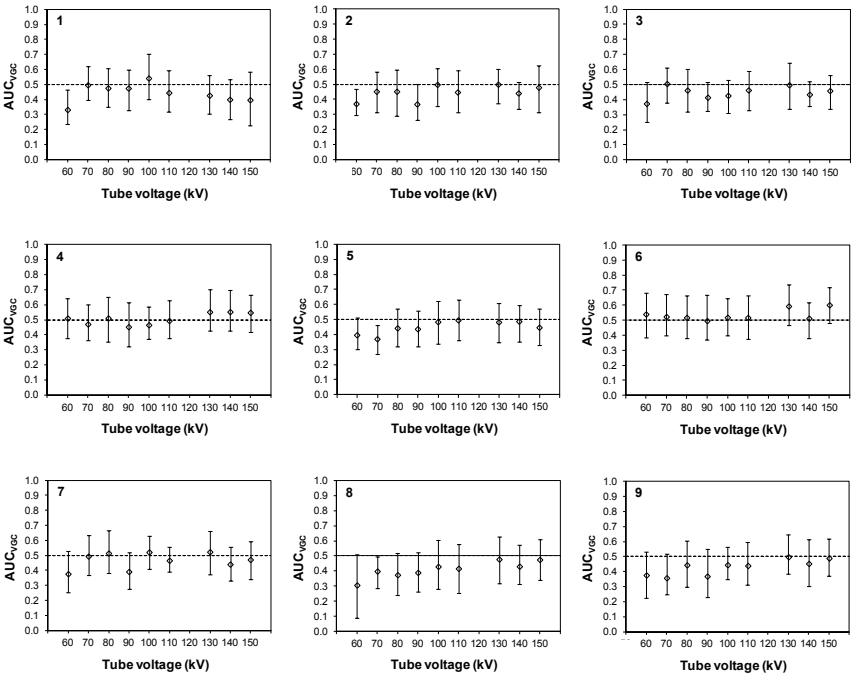

Figure 10: *AUC_{VGC} for each of the image quality criteria for all tube voltages included in Paper I. The image quality criterion is indicated by the number in the top left corner of each plot. Error bars represent the 95% confidence intervals. See Table 2 for a description of the image quality criteria.*

The overall results of the study suggest that, at the default dose level of the VolumeRAD system, the negative effects on image quality resulting from a reduction in number of projection images are not fully compensated by the potential benefits from increasing the dose per projection image. Moreover, the results indicate that the tube voltage used will not have a large impact on image quality. In total, this indicates that the standard setting of the VolumeRAD system, in terms of tube voltage, projection density and angular range, is an optimal configuration at the default dose level.

Paper II: Evaluation of accuracy and precision of manual size measurements in chest tomosynthesis using simulated pulmonary nodules

In Paper II the accuracy and precision of nodule size measurements in chest tomosynthesis images were investigated. Hybrid images consisting of clinical chest tomosynthesis images containing simulated nodules with known sizes were used. As mentioned in Section 4.2, the simulated nodules in Paper II were given a spheroid shape. The volumes of the nodules corresponded to that of a sphere with a diameter of 4, 8 or 12 mm. The direction, in the image plane, of the longest axis of the included nodules varied, ranging from being parallel to the tomosynthesis scan direction to being perpendicular to the scan direction. A circular region of interest (ROI) was inserted in each image to mark the position of the nodules. In Figure 11, cutouts from images included in the study are shown.

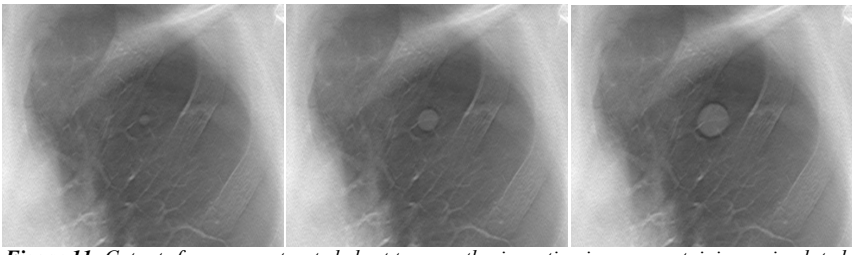

Figure 11*: Cutouts from reconstructed chest tomosynthesis section images containing a simulated nodule included in Paper II. The longest diameter of the nodules from left to right are 4.3mm, 8.6 mm and 12.9 mm.*

A measurement study was conducted in which four thoracic radiologists were given the task of determining the longest diameter of each nodule. The images were displayed with ViewDEX and the observers used the built-in measurement tool. In order to investigate the intraobserver variability, each nodule was measured twice. The observers had the option of stating the nodule as non-measurable if it was deemed not visible or not adequately reproduced for measurement.

A similar mean measurement error, ranging from -0.3 mm to 0.1 mm was found for all observers and nodule sizes. A number of nodules corresponding in volume to a sphere with a diameter of 8 mm or 12 mm positioned in low-signal regions of the projection images, for example behind the heart or the diaphragm, were found to be noticeably underestimated in size (measurement error $\geq$ 1.5 mm). Corresponding regions in the reconstructed tomosynthesis images contain

high levels of quantum noise, as well as substantial out-of-plan residual blur from the heart or the diaphragm hampering the contrast of the nodule borders. The smaller nodules with corresponding locations were stated as non-measurable. In general, nodules in the smallest size group were deemed non-measurable with a higher rate than the larger nodules. The measurement variability, expressed as the standard deviation of the measurement errors, ranged from 0.3 mm to 0.7 mm for all observers and nodule size groups. The intraobserver variability, expressed as the standard deviation of the two measurements on each nodule, averaged over all nodules in each size group, ranged from 0.2 mm to 0.4 mm for all observers. The interobserver variability, expressed as the standard deviation of the measurements by all observers on each nodule, averaged over all nodules in each size group, was 0.2 mm, 0.2 mm and 0.3 mm for the three nodule size groups.

The results of the study suggest a high accuracy and precision for manual measurements of nodules in chest tomosynthesis images. However, nodules with a longest diameter smaller than 5 mm may be difficult to measure at all due to poor visibility. The results also suggest that chest tomosynthesis may not be suitable for follow up of pulmonary nodules in cases where the nodule is located in a region of a section image containing a substantial level of noise and out-of-plane artifacts. It should be kept in mind that the study was performed using simulated nodules with simple spheroid shapes.

Paper III: Effect of radiation dose level on accuracy and precision of manual size measurements in chest tomosynthesis evaluated using simulated pulmonary nodules

Paper II indicated that, for nodules positioned in regions of the chest tomosynthesis images not affected by substantial out-of-plane artifacts or high levels of quantum noise, size measurements in the images can be performed with high accuracy and precision at the standard dose level. In Paper III, the aim was to investigate the possibility of reducing the dose level without impairing the measurement accuracy and precision for nodule with such positions in the lung. Hybrid images, consisting of clinical chest tomosynthesis images containing simulated spheroid-shaped nodules with known sizes, were used. Additionally, two dose reduction simulations were performed for each included image set, resulting in images corresponding to 50% and 32% of the original dose level. As mentioned in Section 4.1, the effective dose to a standard-sized patient resulting from a chest tomosynthesis examination with the default settings of the GE

VolumeRAD system has been determined to 0.12 mSv (170 cm and 70 kg) [4]. Consequently, the simulated dose levels in Paper III corresponded to effective doses of 0.06 and 0.04 mSv to a standard-sized patient. The volumes of the nodules corresponded to that of a sphere with a diameter of 4, 8 or 12 mm. A circular ROI was inserted in the images to mark the position of the nodules. In Figure 12, an example of a nodule at the three different dose levels included in the study is shown.

Four thoracic radiologists participated in a measurement study in which they were given the task of determining the longest diameter of each nodule at each of the three dose levels. The nodules in the three different dose levels were presented to the observers in a random order. In order to investigate the intraobserver variability, the nodules were presented in a second round in new random order. The observers had the option of stating the nodule as non-measurable if it was deemed not visible or not adequately reproduced for measurement. Repeated measures analysis of variance (ANOVA) was used in conjunction with post hoc pairwise comparisons to test the overall effect of dose level on measurement accuracy and precision [110]. The tests were made separately for each nodule size group and observer.

For all observers and dose levels, the mean measurement errors ranged from -0.7 mm to -0.2 mm, -0.4 mm to -0.1 mm, and -0.2 mm to -0.1 mm, respectively, for the smallest, intermediate sized and largest nodules. For two of the observers, a significant decrease in measurement accuracy was found for the lowest dose level as compared to the other two dose levels. For all observers and dose levels, the intraobserver variability, expressed as the standard deviation of the two measurements on each nodule, averaged over all nodules in each size group, ranged from 0.1 mm to 0.3 mm, 0.1 mm to 0.4 mm, and 0.2 mm to 0.4 mm, for the three different nodule size groups. A significant increase in intraobserver variability as compared to the other two dose levels was found for the lowest dose level for one observer. In general, nodules in the smallest size group were deemed non-measurable with a higher rate than the larger nodules.

The results of the study indicate that, for pulmonary nodules at positions in the lungs corresponding to locations in high-signal regions of the projection images, using a radiation dose level resulting in an effective dose of 0.06 mSv to a standard-sized patient may be possible in chest tomosynthesis without affecting the accuracy and precision of nodule diameter measurements to any large extent.

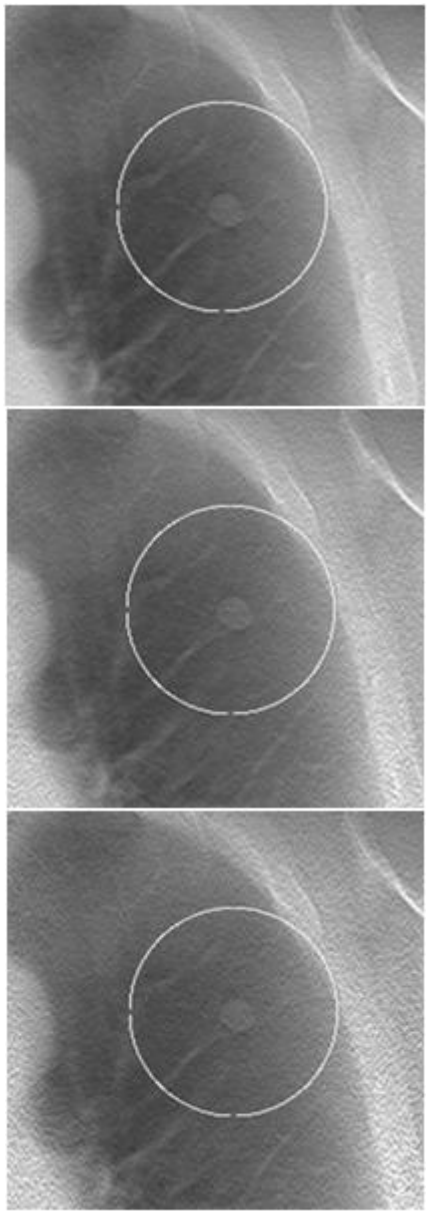

Figure 12: *Cutouts from reconstructed chest tomosynthesis section images included in Paper III, containing a simulated nodule with a longest diameter of 8.9 mm, at the original dose level (top) as well as at a simulated dose level of 50% (middle) and 32% (bottom) of the original dose level.*

Paper IV: Influence of the in-plane artefact in chest tomosynthesis on pulmonary nodule size measurements

In Paper IV, the measurement data generated in Paper II was used to investigate the effect of the in-plane artifact in tomosynthesis images on the accuracy of pulmonary nodule size measurements. As mentioned in the summary of Paper II above, the direction, in the image plane, of the longest axis of the included nodules varied, ranging from being parallel to the tomosynthesis scan direction to being perpendicular to the scan direction. Any association between measurement error and the direction of the longest diameter could thereby be investigated. This was done by using the Kendall rank correlation coefficient, referred to as Kendall's tau [111], with a 5% significance level. The analysis was performed separately for each observer and nodule size group. Additionally, an inquiry of how the radiologists handled the artifact during measurements was made. Figure 13 shows two nodules included in the study.

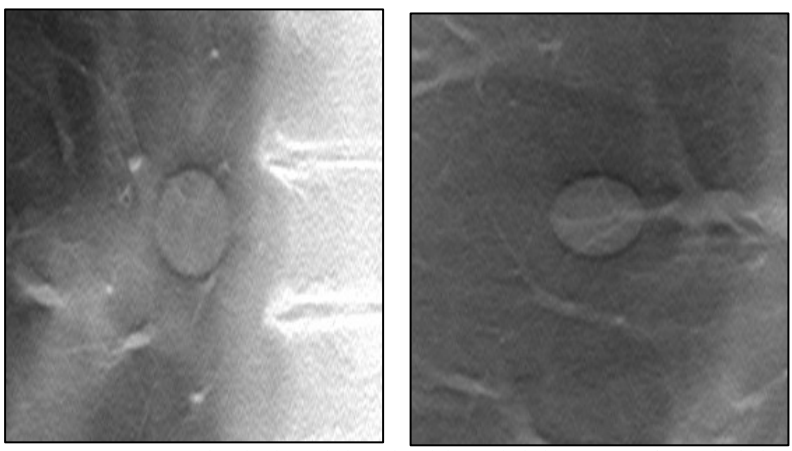

Figure 13*: Two simulated spheroid-shaped nodules included in Paper II from which the measurement results were retrospectively analyzed in Paper IV. The longest diameter of the nodule to the left is parallel to the tomosynthesis scan direction. The longest diameter of the nodule to the right is perpendicular to the scan direction. The in-plane artifact is visible as dark areas around both nodules.*

None of the observers had chosen to include the artifact in their measurements. Values of Kendall's tau for all observers and nodule size groups are presented in Table 3. For two of the observers, significant association between measurement error and the direction of the longest diameter relative to the scan direction was found for the largest nodules. The association was such that the magnitude of the measurement error increased with decreasing angle between the longest diameter and the scan direction.

***Table 3**: Kendall's tau, measuring association between the direction of the longest diameter of the nodule and the measurement error, for all observers and nodule size groups. Significant association, at a 5 % significance level, is indicated by an asterisk.*

	Nodule size group (Range of longest diameters)		
Observer	4.3 - 5.2 mm	8.5 - 10.5 mm	12.8 - 15.7 mm
1	-0.151	0.093	0.324*
2	0.008	0.093	0.147
3	-0.063	0.129	0.200*
4	-0.180	-0.071	0.073

The results indicate that there is a risk of underestimating the size of pulmonary nodules in manual diameter measurements, if the in-plane artifact is omitted in the measurement. However, the effect is minor and of little clinical relevance.

Paper V: Detection of pulmonary growth with chest tomosynthesis: a human observer study using simulated nodules and simulated dose reduction

Paper V investigates the possibility of detecting pulmonary nodule growth over time with chest tomosynthesis. Pairs of clinical chest tomosynthesis examinations were included in the study. The two examinations in each pair were from the same patient, performed at two separate occasions. As mentioned in Section 4.2, simulated nodules with clinically realistic appearances were used in the study. The nodules were divided into two size categories, with volumes of approximately 100 mm^3 and 300 mm^3, in concordance with the lower and upper limit of the range of nodule sizes that would lead to follow up, as suggested by the NELSON trial [45]. Additional versions of the nodules with increasing volumes were also created. The nodules were inserted into the images from the pairs of chest tomosynthesis examinations, simulating cases where the nodule had either remained stable in size or increased in size between the two imaging occasions. A simulated dose reduction was applied to a subset of the cases. The resulting dose-reduced images corresponded to an effective dose of 0.04 mSv for a standard-sized patient. A mismatch of the position of the center of the nodule, relative to the plane of focus in the final reconstructed images, between the two pairs of tomosynthesis examinations was introduced in another subset of cases. In total, four different sets of cases differing in terms of nodule size, included

nodule growths, dose level and nodule position relative to the plane of focus were included. Figure 14 shows examples of nodules from each case set included in the study. See Table 4 for a summary of the included case sets.

***Table 4**: Description of the four sets of chest tomosynthesis examinations included in Paper V.*

Case set	Volume, baseline nodules	Relative nodule volume increase	Dose level (mSv)	Nodule placement
1	245 - 293 mm^3	20%, 68%, 108% and 252%	0.04	Nodule center in plane of focus
2	98 - 146 mm^3	11%, 20%, 37% and 68%	0.12	Nodule center in plane of focus
3	245 - 293 mm^3	11%, 20%, 37% and 108%	0.12	Nodule center in plane of focus
4	98 - 146 mm^3	11%, 20%, 37% and 68%	0.12	Nodule center in plane of focus or in between two planes of focus

Four thoracic radiologists participated in an observer study in which they were presented with the pairs of chest tomosynthesis examinations. The radiologists rated their confidence that the nodules were stable in size or not using a five point rating scale. This was done before any measurements of the nodule sizes were performed, and then again after measurements. Based on the results of their measurements, the radiologists then rated their confidence that there had been a clinically relevant nodule growth or not. The rating data for the nodules that were simulated to be stable in size was compared to the rating data for the nodules simulated to have increased in size using ROC analysis. VGC Analyzer was used to perform the analysis.

Concerning the confidence of nodule growth or not, AUC values ranging from 0.9 to 1 was obtained for nodule growths of 37% or more. For the two smallest growths (11% and 20%), obtained AUC values ranged from 0.65 to 0.93. The lowest AUC values were found for the dose-reduced cases. The results also indicated that the AUC decreased with decreasing baseline nodule size, and if there was a mismatch of the nodule position relative to the plane of focus between the examinations in one pair. For the rating data regarding if there had been a clinically relevant growth or not, and assuming a follow up interval of three months, AUC values ≥ 0.95 were found for nodules with corresponding VDTs of approximately 200 days or less.

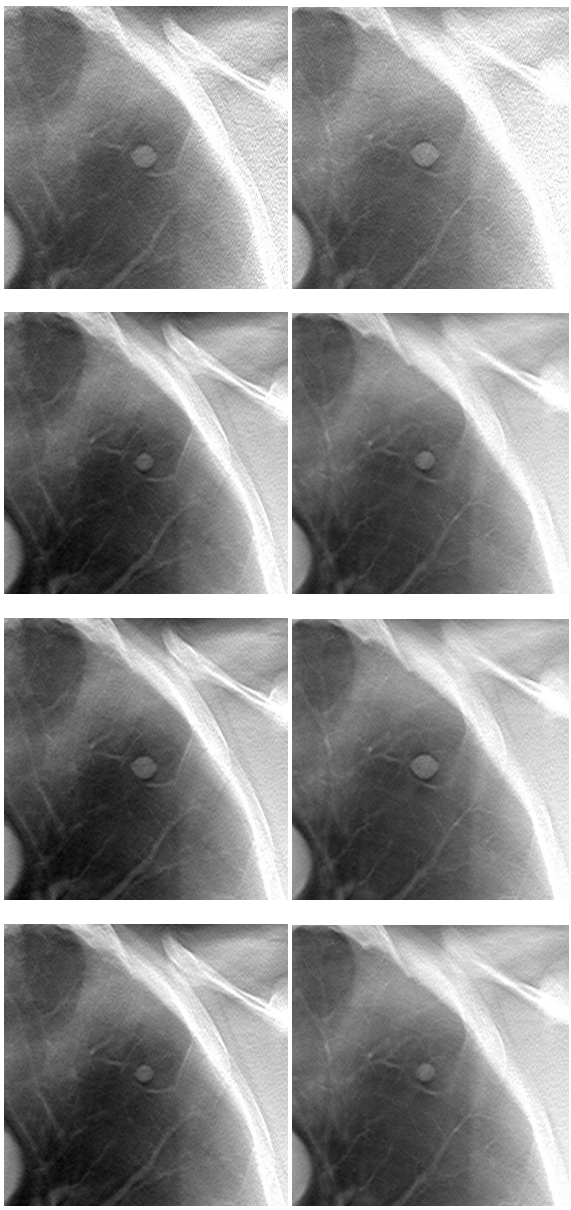

***Figure 14**: Cut outs from chest tomosynthesis images from one included pair of chest tomosynthesis examinations in each of the four case sets included in Paper V. Cut outs are shown from case set 1 to 4 from top to bottom in ascending numerical order. All cases represent a 20% volume increase of the nodule between the left and the right image. In the case shown for case set 4, the center of the nodule is in the plane of focus in the left image while the right image represents a situation where it is in between two planes.*

6. Discussion

This thesis presents studies aiming at investigating the effect of different image acquisition parameters in chest tomosynthesis on perceived image quality and on assessment of pulmonary nodules. Furthermore, the thesis aims at contributing to a general evaluation of the use of chest tomosynthesis for follow up of pulmonary nodules. The image material included in the studies consisted of hybrid images based on images of an anthropomorphic phantom or clinical patient images, to which artificial noise or nodules (or both) have been added. Evaluations were performed by using methods that included participation of experienced thoracic radiologists

The work in this thesis can be seen as following an optimization strategy for radiographic imaging systems as proposed by Båth et al. [112]. This strategy is based on first finding the optimal imaging parameters for a given radiographic system while keeping the effective dose constant. After the optimal imaging parameters have been determined, the optimization process can proceed with determination of the optimal amount of radiation to be used. Furthermore, Båth et al. suggest that the anatomical background should be included in all steps of the optimization process. Paper I can be seen as corresponding to the first step in such a process for chest tomosynthesis. Further, Papers III and V correspond to the second step of determining an optimal dose level, in this case specifically for pulmonary nodule size assessment and for detection of pulmonary nodule growth in chest tomosynthesis. However, one might question the claim of these studies being fully acceptable dose optimization studies. In particularly for Paper V, it would have been preferable, in a dose optimization point of view, to include more dose levels. Nevertheless, the results of the study showed trends that might be valuable for any further evaluation of dose level in chest tomosynthesis. All studies included in this thesis conform to the suggestion of Båth et al. to include the anatomical background in the entire optimization process.

In Paper I, no overall benefit was seen, in terms of perceived image quality, of operating the detector at a higher DQE while reducing the number of acquired projection images of a chest tomosynthesis scan with the GE VolumeRAD system using the standard dose level. It was concluded that the default configuration of 60 projection images acquired within 30° is a good alternative

at this dose level. This configuration has also been recommended for chest tomosynthesis by Machida et al. [39]. Admittedly, the results obtained in Paper I did indicate an improved image quality for decreased angular ranges as compared to the default configuration, for the criteria related to the trachea, large and medium sized vessels and thoracic aorta. However, these results might be a consequence of the image quality criteria resembling, to some extent, those previously described for CXR by the European commission and thereby not fully reflecting the strengths of tomosynthesis over CXR. As the angular range of the tomosynthesis scan is reduced, and the depth resolution in the tomosynthesis images consequently is reduced, the resemblance of the tomosynthesis images to CXR images will to some extent increase. One of the used criteria in Paper I was specifically linked to the depth resolution of the images, namely the criteria regarding the possibility to follow vessels through the volume. For the configurations with decreased angular intervals, this possibility was reduced as compared to the default settings.

In a similar study as that presented in Paper I, Jadidi et al. [113] evaluated the quality of chest tomosynthesis images using the Fujifilm imaging system. They scanned an anthropomorphic phantom, including relevant anatomical structures as well as a spherical structure simulating a nodule, using ten different image acquisition configurations. The angular interval and projection image density of the included configurations ranged, respectively, from 10° to 27° and from 1.5/° to 4.4/°. Thoracic radiologists participated in a visual grading study in order to evaluate the image quality obtained with the different configurations. Image quality criteria regarding the reproduction of the borders of vessels, of the carina, of a vertebral body in the thoracic spine, and of the border of the artificial nodule were included. Additionally, a criterion related to the depth resolution in the images, regarding the disturbance of surrounding nodules on the outlining of a single vessel, was included. VGC analysis was used to evaluate the data. The vendor-recommended configuration, which included an angular interval of 27° and a projection image density of 2.2/°, was used as reference in the analysis. Regarding the effect of the angular interval on the image quality, the results were similar to what was reported in Paper I. For example, for the criterion regarding the disturbance from surrounding vessels, significantly inferior image quality was found for configurations with angular intervals <20°. In terms of reproduction of the carina and the spine, the image quality increased with decreasing angular interval. No strong effect of projection image density on the image quality was however found. As pointed out by Jadidi et al., their study included higher projection image densities then what was the case in Paper I. One alternative configuration, including 32 acquired projection images within

20°, was found to yield similar image quality as the vendor recommended configuration. Jadidi et al. identified the alternative configuration as clinically valuable as it would result in an examination time of 6.3 seconds, which was shorter than for the vendor-recommended configuration (12 seconds). A shortening of the examination time could lower the risk of occurrence of respiratory motion artifacts in the images, as it would make it easier for the patient to hold his or her breath for the duration of the scan.

Regarding the negative effect in Paper I on image quality due to decreasing projection image densities as compared to the default configuration, it was evident that introduced ripple artifacts in the images due to insufficient blurring of out-of-plane structures hampered the reproduction of anatomical structures. In the case of breast tomosynthesis images, methods for reducing out-of-plane artifacts caused by high-density structures such as calcification and metal objects have been proposed [114, 115]. The methods are based on identifying the projection images that will introduce artifacts to a voxel in the reconstructed tomosynthesis image. These projection images can then be rejected in the reconstruction of that voxel. Wu et al. [115] proposed a method for determining sources of ripple artifacts in the image by segmentation of high-contrast objects in the projection images. This technique might also be applicable in chest tomosynthesis by segmenting the ribs in the projection images [116]. As mentioned in Section 3.1, the ribs can be a major source of ripple in chest tomosynthesis images.

The conclusions in Paper I are valid for the GE VolumeRAD system and its implemented FBP reconstruction algorithm. Other acquisition configurations may be optimal for other systems and reconstruction techniques. For example, Godfrey et al. [117] have studied the effect of different image acquisition configurations on the image quality in chest tomosynthesis images reconstructed using a technique referred to as matrix inversion tomosynthesis (MITS) [118]. With MITS, the out-of-plane blur in each tomosynthesis section image resulting from the SSA technique is removed by applying the inverse of a matrix describing the blur to each image. This is performed in the frequency domain. The blurring functions are determined by using knowledge of the geometry of the tomosynthesis system combined with linear systems theory. Godfrey et al. measured the MTF and impulse response resulting from different image acquisition configurations in a tomosynthesis system using MITS for image reconstruction. Additionally, they made visual evaluations of images of an anthropomorphic phantom and of two human subjects. They concluded that the

optimal configuration using their imaging system together with a MITS reconstruction was to acquire 71 projection images within a scan angle of 20°.

As mentioned in Subsection 3.4.3, the use of an anthropomorphic chest phantom instead of clinical patient images in a visual grading study might make one question the clinical validity of the obtained results. In Paper I, a single phantom was used and as such, even though the anatomical complexity of the phantom was high, the study does not take anatomical variations among patients into account. However, to the authors' knowledge, no previous study of the influence of projection image configuration and tube voltage on the quality of chest tomosynthesis section images, evaluated with the use of clinically relevant quality criteria, had been presented prior to Paper I. Therefore, it was decided that the design of Paper I was sufficient for detecting trends that might be guiding in further investigations of the image quality in chest tomosynthesis.

As mentioned previously, Svensson et al. [64] found that, compared to real nodules, simulated nodules generated with the method used in this thesis had a slightly too high detection rate. Svensson et al. discuss the limitations of the simulation method concerning this. In terms of detection studies, they argue that the method might still be valid for studies of relative nature, for example when investigating the effect on detection rate of nodule size or position in the lung. However, when seeking an absolute threshold of detection, the method should be used with caution. For studies aiming at investigating measurement precisions, as those performed in Paper II – V, Svensson et al. argue that the slightly higher detection rate should not be an issue. The results concerning the number of nodules judged as non-measurable in these papers should however be considered as affected by a too high detection rate. Also, as Paper II indicated that the signal, in this case the nodule borders, in relation to the noise might be too low for reliable diameter measurements in low-signal regions in the images, Paper III was restricted to nodules in the high-signal regions. As Svensson et al. showed that the contrast of the simulated nodules was slightly too high in these regions, the identified effect of the dose level on measurement precision might be expected to appear at higher dose levels than what was indicated by Paper III.

In concordance with the discussion given by Svensson et al. [64] considered above, when using simulated pathology in evaluation of medical images, it is important to match the realism of the appearance of the pathology with the aim of the study. To put it differently, it is important to be careful when applying the results of such a study to the clinical situation. In Papers II – IV, the main aim was to evaluate the effect of nodule size and dose level on the absolute accuracy

of pulmonary nodule diameter measurement in chest tomosynthesis images. In this case, the possibility to control the length of the longest diameter of the included nodules was deemed important. This would have been more difficult if the method available for providing the nodules with realistic appearances had been used. Therefore, the results should be seen as a representing a best-case scenario in terms of what is possible with chest tomosynthesis.

In general, the work presented in this thesis suggests that measurements of pulmonary nodule diameters in chest tomosynthesis images can be performed with high accuracy and precision for the range of included nodule sizes (4 – 15 mm). One can assume that the results are applicable also to nodules larger than those included in this thesis. Both measurement accuracy and variability were in the magnitude of a few tenths of a millimeter. Small nodules (< 5.0 mm) were however found to be difficult to measure at all due to low visibility in the images. However, as concluded from results from the NELSON trial [45] and other previous reports [34], nodules in this size category might not require follow up due to low risk of being lung cancer.

The effect of the inherent in-plane artifact in chest tomosynthesis images, visible as dark areas around certain structures, on the accuracy of size measurement of pulmonary nodules was investigated in Paper IV. The study could only show a significant effect on the largest included nodule size group. For the smaller included nodules, other factors, such as difficulties in detecting the nodule borders at all, were probably more prominent in the study. The measurement data used were originally generated in a study not specifically designed for the answering the question at issue in Paper IV. However, due to the range of measurement directions included and the placement of the nodules in clinical anatomical backgrounds, it was judged that relevant results could be obtained.

It should be noted that the conclusions in Paper IV should not be interpreted as it being appropriate to include the artifact when measuring pulmonary nodules. In fact, this would most likely lead to an even larger error in measurement accuracy. Svahn et al. [36] have previously investigated the extent of the artifact in the scan direction, using a phantom with homogenous background containing spheres with four different densities. For each density, five spheres with diameters of 4, 8, 12, 16 and 20 mm were included. Svahn et al. found that the extent of the in-plane artifact, relative to the boundaries of the spheres, ranged from 0.0 mm to up to 6.0 mm. The extent increased with increasing sphere size and contrast.

In Paper V, the radiologists could in general distinguish nodules stable in size over time from nodules showing clinically relevant growth. It should be pointed out that an ideal situation for detecting nodule growth was created in Paper V, as simulated nodules showing symmetrical growth was used. As such, it can be expected that the limitations for nodule growth detection will be greater in clinical cases than what was indicated in Paper V. Nevertheless, the overall results are encouraging for proceeding with the evaluation of the use of chest tomosynthesis for pulmonary nodule follow up.

The strength of Paper V is that it contributes with data that would be difficult to obtain using clinical images. The volumes of the simulated nodules could be controlled, and as such allowed for inclusion of nodule sizes covering the lower and upper limit of the range of sizes that would lead to follow up as suggested by the NELSON trial [45]. Additionally, exact knowledge of the magnitude of growth of the included nodules was achieved, which is perhaps the greatest strength with using simulated nodules in this case. The method for inserting the simulated nodules in the images also allowed for freely choosing the locations of the included nodules in the lung. As such, the possibility of assessing the effect of mismatch of nodule position relative to the plane of focus in the tomosynthesis section images was simplified.

In the clinical situation of pulmonary nodule follow up using chest tomosynthesis, there is a risk of underestimating or overestimating nodule growth if there is a mismatch in nodule position relative to the closest plane of focus between the baseline and follow up examination. In Paper V, the ability to separate nodules stable in size from growing nodules was in general lower for the cases that included a mismatch in position in comparison to corresponding nodules positioned similarly in the baseline and follow up examination. The effect was however small for nodule growths corresponding to a relative increase in volume of 37% or more. In Paper V, the effect was only assessed for the smaller original nodules with volumes of approximately 100 mm^3. It can be assumed that the effect would be smaller for nodules in the larger size group. Juluru et al. [119] have previously showed an inherent variability in measurements of nodule diameter due to the position of the nodule relative to the image slice planes in CT. They used a geometric model including a spherical nodule in a uniform density. A segmentation-based method was used to assess the longest diameter of the nodules. In accordance with the results in Paper V, Juluru et al. found that the variability increased with decreasing nodule size. In Paper V, the images were reconstructed with 5 mm intervals. The effect of the mismatch in nodule position relative to the plane of focus can be reduced by

reconstructing the tomosynthesis section images at smaller intervals. As mentioned in Section 4.1, the GE VolumeRAD imaging system used allows for reconstruction intervals of down to 1 mm.

One might question the inclusion of a dose level of 0.04 mSv in Paper V, since Paper III indicated that using this dose level could affect the intraobserver variability. However, in Paper III, it was concluded that the overall measurement accuracy and precision was high and that the observed effect of dose level might not be clinically relevant. Additionally, Paper III did not specifically study the possibility of detecting size changes. Using a dose level of 0.04 mSv in Paper V was also motivated by the previously mentioned results from Asplund et al. [50], suggesting no significant difference in detection rate of pulmonary nodules between chest tomosynthesis images acquired at 0.04 mSv and at the standard dose level of 0.12 mSv. In Paper V, the lowest AUC values were found for the cases that corresponded to a dose level of 0.04 mSv. However, the design of the study and the choice of method for data analysis made significance testing between the dose levels difficult.

Gavrielides et al. [86] performed a study, similar in design to Paper V, evaluating segmentation-based volumetric measurements in CT for use in detection of pulmonary nodule growth. They used an anthropomorphic chest phantom including artificial nodules. Four different nodule shapes (spherical, elliptical, lobulated, and speculated) were included. For each shape, four different volumes were included: 65 mm^3, 268 mm^3, 382 mm^3 and 524 mm^3. The study showed that, looking at all nodule shapes, an AUC level of 0.95 was achievable for a volume change of $\leq$20%, indicating a superior sensitivity for CT as compared to the results in Paper V. The results of Gavrielides et al. also indicated decreasing AUC values with decreasing nodule size, similar to what was seen in Paper V for chest tomosynthesis. It should however be noted that the results from Gavrielides et al. are based on distributions of nodule measurements of one nodule at a time, while Paper V is based on distributions of volume change measurements from pairs of nodules. As such, it is not obvious if the results from the two studies are directly comparable. Other studies based on clinical nodules have shown that variability in nodule volume measurements in CT is in the range 22% to 25% [92, 95, 97]. However, these studies are based on variability measurements on nodules stable in size. As mentioned in Subsection 3.4.2, such studies do not include the ability of the radiologist to take perceived nodule size-change into account and the sensitivity in the clinical situation might therefore be underestimated. Nevertheless, recommendations concerning the use of CT in the follow up of pulmonary nodules state that a 25% relative volume

increase is required for a nodule growth to be considered as significant [35]. Even though, as stated above, one should be careful with applying the absolute results from Paper V to the clinical situation, the results do suggest that a similar cut off may be reasonable for chest tomosynthesis as well. However, further studies, preferably including clinical cases, should be performed to assess such a specific limit for chest tomosynthesis.

Automated volumetric measurements of nodule size have been shown to be more sensitive than 2D diameter measurements in terms of detecting nodule growth in CT images [120, 121]. Due to the limited angle of a chest tomosynthesis scan, there will be anisotropy in terms of resolution in the imaged volume [122], restricting nodule size measurements to only one plane. This is of course a limitation of chest tomosynthesis regarding its use in pulmonary nodule follow up. In assessment of pulmonary nodules, size measurements are an important help for the radiologists. However, as mentioned previously, they will also take perceived nodule size change into account when judging if any size change of the nodule has occurred [103].

In recent studies [101, 123], it has been concluded that CT performed at a sub-mSv dose level and even at as low a level as that of a chest tomosynthesis examination performed with the VolumeRAD system, can be used for pulmonary nodule follow up. This was concluded since it was shown that nodule detection sensitivity and volumetric measurement accuracy were on clinically acceptable levels. Considering the use of chest tomosynthesis as an alternative to chest CT might therefore not solely be a question of reduction of dose. As tomosynthesis systems are modified radiography or fluoroscopy systems, advantages of chest tomosynthesis also include the relative simplicity of the technique. In general, the possibility of adding a tomosynthesis examination in direct conjunction to a CXR, as mentioned in Subsection 3.3.2, has been identified as one of the major advantages in terms of clinical use for the technique. Additionally, it should be noted that the role of chest tomosynthesis in the clinical thoracic radiology practice is linked to the other available imaging resources [53]. For example, at clinics with limitations in CT resources, the use of chest tomosynthesis instead of certain clinical tasks could be a way to optimize the use of the CT resources.

7. Conclusions

Specific conclusions drawn from the work presented in this thesis are:

- For a standard-sized patient and at the standard dose level of the VolumeRAD tomosynthesis imaging system, potential benefits in terms of perceived image quality of increasing the dose per projection image do not fully compensate for the negative effects of an accompanying reduction in number of acquired projection images. Consequently, the default configuration of 60 acquired projection images within 30° is a good alternative. The tube voltage used for a chest tomosynthesis examination does not have a large impact on perceived image quality.

- Measurements of the diameter of pulmonary nodules in chest tomosynthesis images may be performed with high accuracy and precision. However, small nodules (< 5.0 mm) can be difficult to measure at all due to low visibility in the images.

- A dose level resulting in an effective dose of 0.06 mSv to a standard-sized patient may be possible in chest tomosynthesis without affecting the accuracy and precision of diameter measurements of pulmonary nodules with positions in the lung corresponding to high-signal regions in chest tomosynthesis projection images. For low-signal regions, the accuracy is hampered even at the original dose-level due to that these regions correspond to regions in the section images containing substantial noise and out-of-plane artifacts.

- There is a risk of underestimating the size of a pulmonary nodule if the in-plane artefact—visible as darker areas around pulmonary nodules—is omitted from manual diameter measurements in chest tomosynthesis images. However, the effect is minor and of little clinical relevance. Including the artifact would most likely result in an even larger measurement error.

- Chest tomosynthesis is a promising imaging modality for detection of pulmonary nodule growth. However, a number of factors that may affect the

sensitivity was identified. The possibility to detect growth may decrease with decreasing nodule sizes. Mismatch in nodule position relative to the plane of focus between two consecutive chest tomosynthesis examinations can also hamper the detection. Finally, using a dose level corresponding to an effective dose of 0.04 mSv may affect the detection in a negative manner.

8. Future perspectives

A suitable continuation of the work of optimizing image acquisition parameters in chest tomosynthesis with the VolumeRAD system would be to investigate the effect of a general dose reduction, still using the default configuration, on perceived image quality. Preferably, this would be done using clinical images together with a simulated dose reduction. If such a study would support a reduction in dose, a study similar to the one in Paper I could be of value to repeat at this lower dose level. This is partly due to that the dependency of DQE on the dose level is stronger at lower dose levels and that the influence of the noise will be stronger compared to other disturbing components [124].

The results of the studies evaluating nodule size assessment presented in this thesis should be followed with studies using clinical chest tomosynthesis images. For example, cases containing real nodules which have been proven stable over a substantial period of time could be used to investigate clinical measurement variability. This could be combined with a simulated dose reduction technique to look at the effect of the dose level.

As mentioned previously, in the case of CT imaging, volumetric measurements of nodules have been proven more reliable than 2D diameter measurements. Methods for adding a second view of a tomosynthesis scan have been shown to result in a more isotropic volume rendition [122, 125]. Future work could investigate the possibility for volumetric nodule measurements using these methods. Of course, this would add to the examination time and complexity of the examination, perhaps limiting some of the advantages over CT. However, as mentioned in Chapter 6, chest tomosynthesis could still be a valuable tool for optimizing the use of other imaging modalities.

Acknowledgements

This work was supported by grants from the Swedish research council; the Swedish Radiation Safety Authority; the Swedish state, under the agreement between the Swedish government and the county councils concerning the economic support of research and education of doctors (ALF agreement); and the Healthcare sub-committee, Region Västra Götaland (Hälso- och sjukvårdsutskottet).

I would like to express my sincere gratitude to

My supervisor Magnus Båth, for giving me the opportunity to be part of the tomosynthesis research group at Sahlgrenska University Hospital, for investing time in me, and for the excellent guidance throughout these graduate studies.

My co-supervisors Åse Allansdotter Johnsson, Lars Gunnar Månsson and Angelica Svalkvist for valuable support and for sharing with me your great knowledge in this research area.

My co-authors and research group colleagues:
David Molnar, Rauni Rossi Norrlund and Jenny Vikgren for all the time you have spent visually grading and measuring nodules.
Maral Mirzai for assistance in preparing image material.
Sara Asplund for great cooperation.

Glenn Alfredsson, Mikael Bramer and Johan Fors for facilitating the collection of image material, for setting up the image-reconstruction workstation in my office, and for calibration of monitors.

My co-members of the LETStudio, especially Jonas Ivarsson, Hans Rystedt and Sanna Rimpläinen, for great collaboration.

Patrik Sund for monitor support.

Jonny Hansson for VGC support.

My colleagues for making the Department of Radiation Physics a great workplace. Thanks especially to my PhD-student colleagues for all the fun (and hard work) with DrÄG.

Everyone in the DSF-corridor for great input on my work during RALF-meetings, and for the nice times at Fredagsfrukost.

Erik Pettersson and Peter Bonn for being awesome roommates.

My friends, just for being you, and for being there. (Anna, thanks for proofreading this thesis.)

Mamma Merle, Pappa Olle, and Peter with family for supporting me, in every possible way ♥ (Mom, thanks for the artistic contribution to this thesis.)

References

1. McAdams HP, Samei E, Dobbins J, 3rd, Tourassi GD, Ravin CE. *Recent advances in chest radiography*. Radiology 2006;241:663-683.
2. Mettler FA, Jr., Huda W, Yoshizumi TT, Mahesh M. *Effective doses in radiology and diagnostic nuclear medicine: a catalog*. Radiology 2008;248:254-263.
3. Sabol JM. *A Monte Carlo estimation of effective dose in chest tomosynthesis*. Med Phys 2009;36:5480-5487.
4. Båth M, Svalkvist A, von Wrangel A, Rismyhr-Olsson H, Cederblad Å. *Effective dose to patients from chest examinations with tomosynthesis*. Radiat Prot Dosimetry 2010;139:153-158.
5. Yamada Y, Jinzaki M, Hasegawa I, Shiomi E, Sugiura H, Abe T, Sato Y, Kuribayashi S, Ogawa K. *Fast scanning tomosynthesis for the detection of pulmonary nodules: diagnostic performance compared with chest radiography, using multidetector-row computed tomography as the reference*. Invest Radiol 2011;46:471-477.
6. Yamada Y, Jinzaki M, Hashimoto M, Shiomi E, Abe T, Kuribayashi S, Ogawa K. *Tomosynthesis for the early detection of pulmonary emphysema: diagnostic performance compared with chest radiography, using multidetector computed tomography as reference*. Eur Radiol 2013;23:2118-2126.
7. Dobbins JT, 3rd, McAdams HP, Sabol JM, Chakraborty DP, Kazerooni EA, Reddy GP, Vikgren J, Båth M. *Multi-Institutional Evaluation of Digital Tomosynthesis, Dual-Energy Radiography, and Conventional Chest Radiography for the Detection and Management of Pulmonary Nodules*. Radiology 2016; DOI:10.1148/radiol.2016150497
8. Samei E, Flynn MJ, Eyler WR. *Detection of subtle lung nodules: relative influence of quantum and anatomic noise on chest radiographs*. Radiology 1999;213:727-734.
9. Samei E, Flynn MJ, Peterson E, Eyler WR. *Subtle lung nodules: influence of local anatomic variations on detection*. Radiology 2003;228:76-84.
10. Båth M, Håkansson M, Börjesson S, Kheddache S, Grahn A, Ruschin M, Tingberg A, Mattsson S, Månsson LG. *Nodule detection in digital chest radiography: introduction to the RADIUS chest trial*. Radiat Prot Dosimetry 2005;114:85-91.
11. Håkansson M, Båth M, Börjesson S, Kheddache S, Flinck A, Ullman G, Månsson LG. *Nodule detection in digital chest radiography: effect of nodule location*. Radiat Prot Dosimetry 2005;114:92-96.

12. Håkansson M, Båth M, Börjesson S, Kheddache S, Johnsson AA, Månsson LG. *Nodule detection in digital chest radiography: effect of system noise*. Radiat Prot Dosimetry 2005;114:97-101.
13. Båth M, Håkansson M, Börjesson S, Kheddache S, Grahn A, Bochud FO, Verdun FR, Månsson LG. *Nodule detection in digital chest radiography: part of image background acting as pure noise*. Radiat Prot Dosimetry 2005;114:102-108.
14. Båth M, Håkansson M, Börjesson S, Hoeschen C, Tischenko O, Kheddache S, Vikgren J, Månsson LG. *Nodule detection in digital chest radiography: effect of anatomical noise*. Radiat Prot Dosimetry 2005;114:109-113.
15. Håkansson M, Båth M, Börjesson S, Kheddache S, Grahn A, Ruschin M, Tingberg A, Mattsson S, Månsson LG. *Nodule detection in digital chest radiography: summary of the RADIUS chest trial*. Radiat Prot Dosimetry 2005;114:114-120.
16. Kordolaimi SD, Argentos S, Pantos I, Kelekis NL, Efstathopoulos EP. *A new era in computed tomographic dose optimization: the impact of iterative reconstruction on image quality and radiation dose*. J Comput Assist Tomogr 2013;37:924-931.
17. Kim EY, Chung MJ, Lee HY, Koh WJ, Jung HN, Lee KS. *Pulmonary mycobacterial disease: diagnostic performance of low-dose digital tomosynthesis as compared with chest radiography*. Radiology 2010;257:269-277.
18. Kumar SG, Garg MK, Khandelwal N, Gupta P, Gupta D, Aggarwal AN, Bansal SC. *Role of digital tomosynthesis and dual energy subtraction digital radiography in detecting pulmonary nodules*. Eur J Radiol 2015;84:1383-1391.
19. Galea A, Adlan T, Gay D, Roobottom C, Dubbins P, Riordan R. *Comparison of digital tomosynthesis and chest radiography for the detection of noncalcified pulmonary and hilar lesions*. J Thorac Imaging 2015;30:328-335.
20. Langer SG, Graner BD, Schueler BA, Fetterly KA, Kofler JM, Mandrekar JN, Bartholmai BJ. *Sensitivity of Thoracic Digital Tomosynthesis (DTS) for the Identification of Lung Nodules*. J Digit Imaging 2016;29:141-147.
21. Dobbins JT, 3rd, Godfrey DJ. *Digital x-ray tomosynthesis: current state of the art and clinical potential*. Phys Med Biol 2003;48:R65-106.
22. Dobbins JT, 3rd, McAdams HP, Godfrey DJ, Li CM. *Digital tomosynthesis of the chest*. J Thorac Imaging 2008;23:86-92.
23. Dobbins JT, 3rd. *Tomosynthesis imaging: at a translational crossroads*. Med Phys 2009;36:1956-1967.
24. Dobbins JT, 3rd, McAdams HP. *Chest tomosynthesis: technical principles and clinical update*. Eur J Radiol 2009;72:244-251.
25. Johnsson ÅA, Vikgren J, Svalkvist A, Zachrisson S, Flinck A, Boijsen M, Kheddache S, Månsson LG, Båth M. *Overview of two years of*

clinical experience of chest tomosynthesis at Sahlgrenska University Hospital. Radiat Prot Dosimetry 2010;139:124-129.
26. Johnsson ÅA, Vikgren J, Båth M. *Chest tomosynthesis: technical and clinical perspectives*. Semin Respir Crit Care Med 2014;35:17-26.
27. Jung HN, Chung MJ, Koo JH, Kim HC, Lee KS. *Digital tomosynthesis of the chest: utility for detection of lung metastasis in patients with colorectal cancer*. Clin Radiol 2012;67:232-238.
28. Hwang HS, Chung MJ, Lee KS. *Digital tomosynthesis of the chest: comparison of patient exposure dose and image quality between standard default setting and low dose setting*. Korean J Radiol 2013;14:525-531.
29. Quaia E, Baratella E, Poillucci G, Gennari AG, Cova MA. *Diagnostic impact of digital tomosynthesis in oncologic patients with suspected pulmonary lesions on chest radiography*. Eur Radiol 2016;26:2837-2844.
30. Quaia E, Baratella E, Cioffi V, Bregant P, Cernic S, Cuttin R, Cova MA. *The value of digital tomosynthesis in the diagnosis of suspected pulmonary lesions on chest radiography: analysis of diagnostic accuracy and confidence*. Acad Radiol 2010;17:1267-1274.
31. Quaia E, Baratella E, Cernic S, Lorusso A, Casagrande F, Cioffi V, Cova MA. *Analysis of the impact of digital tomosynthesis on the radiological investigation of patients with suspected pulmonary lesions on chest radiography*. Eur Radiol 2012;22:1912-1922.
32. Quaia E, Baratella E, Poillucci G, Kus S, Cioffi V, Cova MA. *Digital tomosynthesis as a problem-solving imaging technique to confirm or exclude potential thoracic lesions based on chest X-ray radiography*. Acad Radiol 2013;20:546-553.
33. Vikgren J, Zachrisson S, Svalkvist A, Johnsson AÅ, Boijsen M, Flinck A, Kheddache S, Båth M. *Comparison of chest tomosynthesis and chest radiography for detection of pulmonary nodules: human observer study of clinical cases*. Radiology 2008;249:1034-1041.
34. MacMahon H, Austin JH, Gamsu G, Herold CJ, Jett JR, Naidich DP, Patz EF, Jr., Swensen SJ. *Guidelines for management of small pulmonary nodules detected on CT scans: a statement from the Fleischner Society*. Radiology 2005;237:395-400.
35. Callister ME, Baldwin DR, Akram AR, Barnard S, Cane P, Draffan J, Franks K, Gleeson F, Graham R, Malhotra P, Prokop M, Rodger K, Subesinghe M, Waller D, Woolhouse I. *British Thoracic Society guidelines for the investigation and management of pulmonary nodules*. Thorax 2015;70 Suppl 2:ii1-ii54.
36. Svahn T, Ruschin M, Hemdal B, Nyhlén L, Andersson I, Timberg P, Mattsson S, Tingberg A. *In-plane artifacts in breast tomosynthesis quantified with a novel contrast-detail phantom*. Proc. of SPIE 2007; 6510:65104R-1-65104R-12.
37. Tingberg A. *X-ray tomosynthesis: a review of its use for breast and chest imaging*. Radiat Prot Dosimetry 2010;139:100-107.

38. Ziedses des Plantes BG. *Eine neue methode zur differenzierung in der roentgenographie (planigraphie)*. Acta Radiol 1932;13:182-192.
39. Machida H, Yuhara T, Mori T, Ueno E, Moribe Y, Sabol JM. *Optimizing parameters for flat-panel detector digital tomosynthesis*. Radiographics 2010;30:549-562.
40. Hansell DM, Bankier AA, MacMahon H, McLoud TC, Muller NL, Remy J. *Fleischner Society: glossary of terms for thoracic imaging*. Radiology 2008;246:697-722.
41. Erasmus JJ, Connolly JE, McAdams HP, Roggli VL. *Solitary pulmonary nodules: Part I. Morphologic evaluation for differentiation of benign and malignant lesions*. Radiographics 2000;20:43-58.
42. Wahidi MM, Govert JA, Goudar RK, Gould MK, McCrory DC. *Evidence for the treatment of patients with pulmonary nodules: when is it lung cancer?: ACCP evidence-based clinical practice guidelines (2nd edition)*. Chest 2007;132:94S-107S.
43. Hall WB, Truitt SG, Scheunemann LP, Shah SA, Rivera MP, Parker LA, Carson SS. *The prevalence of clinically relevant incidental findings on chest computed tomographic angiograms ordered to diagnose pulmonary embolism*. Arch Intern Med 2009;169:1961-1965.
44. Aberle DR, Adams AM, Berg CD, Black WC, Clapp JD, Fagerstrom RM, Gareen IF, Gatsonis C, Marcus PM, Sicks JD. *Reduced lung-cancer mortality with low-dose computed tomographic screening*. N Engl J Med 2011;365:395-409.
45. Horeweg N, van Rosmalen J, Heuvelmans MA, van der Aalst CM, Vliegenthart R, Scholten ET, ten Haaf K, Nackaerts K, Lammers JW, Weenink C, Groen HJ, van Ooijen P, de Jong PA, de Bock GH, Mali W, de Koning HJ, Oudkerk M. *Lung cancer probability in patients with CT-detected pulmonary nodules: a prespecified analysis of data from the NELSON trial of low-dose CT screening*. Lancet Oncol 2014;15:1332-1341.
46. Vult von Steyern K, Björkman-Burtscher I, Geijer M. *Tomosynthesis in pulmonary cystic fibrosis with comparison to radiography and computed tomography: a pictorial review*. Insights Imaging 2012;3:81-89.
47. Kim EY, Chung MJ, Choe YH, Lee KS. *Digital tomosynthesis for aortic arch calcification evaluation: performance comparison with chest radiography with CT as the reference standard*. Acta Radiol 2012;53:17-22.
48. Lee G, Jeong YJ, Kim KI, Song JW, Kang DM, Kim YD, Lee JW. *Comparison of chest digital tomosynthesis and chest radiography for detection of asbestos-related pleuropulmonary disease*. Clin Radiol 2013;68:376-382.
49. Choo JY, Lee KY, Yu A, Kim JH, Lee SH, Choi JW, Kang EY, Oh YW. *A comparison of digital tomosynthesis and chest radiography in evaluating airway lesions using computed tomography as a reference*. Eur Radiol 2016;26:3147-3154.

50. Asplund SA, Johnsson ÅA, Vikgren J, Svalkvist A, Flinck A, Boijsen M, Fisichella VA, Månsson LG, Båth M. *Effect of radiation dose level on the detectability of pulmonary nodules in chest tomosynthesis*. Eur Radiol 2014;24:1529-1536.
51. Asplund S, Johnsson ÅA, Vikgren J, Svalkvist A, Boijsen M, Fisichella V, Flinck A, Wiksell A, Ivarsson J, Rystedt H, Månsson LG, Kheddache S, Båth M. *Learning aspects and potential pitfalls regarding detection of pulmonary nodules in chest tomosynthesis and proposed related quality criteria*. Acta Radiol 2011;52:503-512.
52. Doo KW, Kang EY, Yong HS, Ham SY, Lee KY, Choo JY. *Comparison of chest radiography, chest digital tomosynthesis and low dose MDCT to detect small ground-glass opacity nodules: an anthropomorphic chest phantom study*. Eur Radiol 2014;24:3269-3276.
53. Johnsson ÅA, Vikgren J, Båth M. *A retrospective study of chest tomosynthesis as a tool for optimizing the use of computed tomography resources and reducing patient radiation exposure*. Acad Radiol 2014;21:1427-1433.
54. Petersson C, Båth M, Vikgren J, Johnsson ÅA. *An analysis of the potential role of chest tomosynthesis in optimising imaging resources in thoracic radiology*. Radiat Prot Dosimetry 2016;169:165-170.
55. Lee KH, Goo JM, Lee SM, Park CM, Bahn YE, Kim H, Song YS, Hwang EJ. *Digital tomosynthesis for evaluating metastatic lung nodules: nodule visibility, learning curves, and reading times*. Korean J Radiol 2015;16:430-439.
56. Dobbins JT, 3rd, McAdams HP, Song JW, Li CM, Godfrey DJ, DeLong DM, Paik SH, Martinez-Jimenez S. *Digital tomosynthesis of the chest for lung nodule detection: interim sensitivity results from an ongoing NIH-sponsored trial*. Med Phys 2008;35:2554-2557.
57. Johnsson ÅA, Svalkvist A, Vikgren J, Boijsen M, Flinck A, Kheddache S, Båth M. *A phantom study of nodule size evaluation with chest tomosynthesis and computed tomography*. Radiat Prot Dosimetry 2010;139:140-143.
58. Johnsson ÅA, Fagman E, Vikgren J, Fisichella VA, Boijsen M, Flinck A, Kheddache S, Svalkvist A, Båth M. *Pulmonary nodule size evaluation with chest tomosynthesis*. Radiology 2012;265:273-282.
59. Rusinek H, Naidich DP, McGuinness G, Leitman BS, McCauley DI, Krinsky GA, Clayton K, Cohen H. *Pulmonary nodule detection: low-dose versus conventional CT*. Radiology 1998;209:243-249.
60. Punwani S, Zhang J, Davies W, Greenhalgh R, Humphries P. *Paediatric CT: the effects of increasing image noise on pulmonary nodule detection*. Pediatr Radiol 2008;38:192-201.
61. Guo W, Li Q, Boyce SJ, McAdams HP, Shiraishi J, Doi K, Samei E. *A computerized scheme for lung nodule detection in multiprojection chest radiography*. Med Phys 2012;39:2001-2012.

62. Svalkvist A, Håkansson M, Ullman G, Båth M. *Simulation of lung nodules in chest tomosynthesis*. Radiat Prot Dosimetry 2010;139:130-139.
63. Svalkvist A, Johnsson ÅA, Vikgren J, Håkansson M, Ullman G, Boijsen M, Fisichella V, Flinck A, Molnar D, Månsson LG, Båth M. *Evaluation of an improved method of simulating lung nodules in chest tomosynthesis*. Acta Radiol 2012;53:874-884.
64. Svensson F, Söderman C, Svalkvist A, Rossi Norrlund R, Vikgren J, Johnsson ÅA, Båth M. *Evaluation of a corrected implementation of a method of simulating pulmonary nodules in chest tomosynthesis*. Acta Radiol 2016; DOI:10.1177/0284185116654330
65. Saunders RS, Jr., Samei E. *A method for modifying the image quality parameters of digital radiographic images*. Med Phys 2003;30:3006-3017.
66. Båth M, Håkansson M, Tingberg A, Månsson LG. *Method of simulating dose reduction for digital radiographic systems*. Radiat Prot Dosimetry 2005;114:253-259.
67. Li CM, Dobbins III JT. *Methodology for determining dose reduction for chest tomosynthesis*. Proc. of SPIE 2007; 6510:65102D-1-65102D-10.
68. Veldkamp WJ, Kroft LJ, van Delft JP, Geleijns J. *A technique for simulating the effect of dose reduction on image quality in digital chest radiography*. J Digit Imaging 2009;22:114-125.
69. Svalkvist A, Båth M. *Simulation of dose reduction in tomosynthesis*. Med Phys 2010;37:258-269.
70. Båth M. *Evaluating imaging systems: practical applications*. Radiat Prot Dosimetry 2010;139:26-36.
71. Chakraborty DP. *New developments in observer performance methodology in medical imaging*. Semin Nucl Med 2011;41:401-418.
72. Månsson LG. *Methods for the evaluation of image quality: a review*. Radiat Prot Dosimetry 2000;90:89-99.
73. Smedby Ö, Fredrikson M. *Visual grading regression: analysing data from visual grading experiments with regression models*. Br J Radiol 2010;83:767-775.
74. Smedby Ö, Fredrikson M, De Geer J, Sandborg M. *Visual grading regression with random effects*. Proc. of SPIE 2012; 8318:831805-1-831805-5.
75. Smedby Ö, Fredrikson M, De Geer J, Borgen L, Sandborg M. *Quantifying the potential for dose reduction with visual grading regression*. Br J Radiol 2013;86:31197714.
76. Saffari SE, Love A, Fredrikson M, Smedby Ö. *Regression models for analyzing radiological visual grading studies--an empirical comparison*. BMC Med Imaging 2015;15:49.
77. Båth M, Månsson LG. *Visual grading characteristics (VGC) analysis: a non-parametric rank-invariant statistical method for image quality evaluation*. Br J Radiol 2007;80:169-176.

78. Båth M, Hansson J. *VGC Analyzer: a software for statistical analysis of fully crossed multiple-reader multiple-case visual grading characteristics studies*. Radiat Prot Dosimetry 2016;169:46-53.
79. Hansson J, Månsson LG, Båth M. *The validity of using ROC software for analysing visual grading characteristic data: an invetigation based on the novel software VCG Analyzer*. Radiat Prot Dosimetry 2016;169:54-59.
80. *European guidelines on quality criteria for diagnostic radiographic images. Report EUR 16260 EN.* 1996, Commission of the European Communities: Luxembourg: Office for official publications of the European Communities.
81. *European guidelines on quality criteria for computed tomography. Report EUR 16262 EN.* 1999, Commission of the European Communities: Luxembourg: Office for official publications of the European Communities.
82. Yankelevitz DF, Gupta R, Zhao B, Henschke CI. *Small pulmonary nodules: evaluation with repeat CT--preliminary experience*. Radiology 1999;212:561-566.
83. Yankelevitz DF, Reeves AP, Kostis WJ, Zhao B, Henschke CI. *Small pulmonary nodules: volumetrically determined growth rates based on CT evaluation*. Radiology 2000;217:251-256.
84. Nietert PJ, Ravenel JG, Leue WM, Miller JV, Taylor KK, Garrett-Mayer ES, Silvestri GA. *Imprecision in automated volume measurements of pulmonary nodules and its effect on the level of uncertainty in volume doubling time estimation*. Chest 2009;135:1580-1587.
85. Willemink MJ, Leiner T, Budde RP, de Kort FP, Vliegenthart R, van Ooijen PM, Oudkerk M, de Jong PA. *Systematic error in lung nodule volumetry: effect of iterative reconstruction versus filtered back projection at different CT parameters*. AJR Am J Roentgenol 2012;199:1241-1246.
86. Gavrielides MA, Li Q, Zeng R, Myers KJ, Sahiner B, Petrick N. *Minimum detectable change in lung nodule volume in a phantom CT study*. Acad Radiol 2013;20:1364-1370.
87. Petrick N, Kim HJ, Clunie D, Borradaile K, Ford R, Zeng R, Gavrielides MA, McNitt-Gray MF, Lu ZQ, Fenimore C, Zhao B, Buckler AJ. *Comparison of 1D, 2D, and 3D nodule sizing methods by radiologists for spherical and complex nodules on thoracic CT phantom images*. Acad Radiol 2014;21:30-40.
88. Gavrielides MA, Li Q, Zeng R, Gong Q, Myers K, Sahiner B, Petrick N. *Detectable change of lung nodule volume with CT in a phantom study with high and low signal to background contrast*. Proc. of SPIE 2016; 9798:978329-1-978329-8.
89. Sun S, Rubin GD, Paik D, Steiner RM, Zhuge F, Napel S. *Registration of lung nodules using a semi-rigid model: method and preliminary results*. Med Phys 2007;34:613-626.

90. Funaki A, Ohkubo M, Wada S, Murao K, Matsumoto T, Niizuma S. *Application of CT-PSF-based computer-simulated lung nodules for evaluating the accuracy of computer-aided volumetry*. Radiol Phys Technol 2012;5:166-171.
91. Young S, Kim HJ, Ko MM, Ko WW, Flores C, McNitt-Gray MF. *Variability in CT lung-nodule volumetry: Effects of dose reduction and reconstruction methods*. Med Phys 2015;42:2679-2689.
92. Wormanns D, Kohl G, Klotz E, Marheine A, Beyer F, Heindel W, Diederich S. *Volumetric measurements of pulmonary nodules at multi-row detector CT: in vivo reproducibility*. Eur Radiol 2004;14:86-92.
93. Revel MP, Bissery A, Bienvenu M, Aycard L, Lefort C, Frija G. *Are two-dimensional CT measurements of small noncalcified pulmonary nodules reliable?* Radiology 2004;231:453-458.
94. Gietema HA, Wang Y, Xu D, van Klaveren RJ, de Koning H, Scholten E, Verschakelen J, Kohl G, Oudkerk M, Prokop M. *Pulmonary nodules detected at lung cancer screening: interobserver variability of semiautomated volume measurements*. Radiology 2006;241:251-257.
95. Gietema HA, Schaefer-Prokop CM, Mali WP, Groenewegen G, Prokop M. *Pulmonary nodules: Interscan variability of semiautomated volume measurements with multisection CT-influence of inspiration level, nodule size, and segmentation performance*. Radiology 2007;245:888-894.
96. Petrou M, Quint LE, Nan B, Baker LH. *Pulmonary nodule volumetric measurement variability as a function of CT slice thickness and nodule morphology*. AJR Am J Roentgenol 2007;188:306-312.
97. de Hoop B, Gietema H, van Ginneken B, Zanen P, Groenewegen G, Prokop M. *A comparison of six software packages for evaluation of solid lung nodules using semi-automated volumetry: what is the minimum increase in size to detect growth in repeated CT examinations*. Eur Radiol 2009;19:800-808.
98. Wang Y, de Bock GH, van Klaveren RJ, van Ooyen P, Tukker W, Zhao Y, Dorrius MD, Proenca RV, Post WJ, Oudkerk M. *Volumetric measurement of pulmonary nodules at low-dose chest CT: effect of reconstruction setting on measurement variability*. Eur Radiol 2010;20:1180-1187.
99. de Jong PA, Leiner T, Lammers JW, Gietema HA. *Can low-dose unenhanced chest CT be used for follow-up of lung nodules?* AJR Am J Roentgenol 2012;199:777-780.
100. Zhao YR, van Ooijen PM, Dorrius MD, Heuvelmans M, de Bock GH, Vliegenthart R, Oudkerk M. *Comparison of three software systems for semi-automatic volumetry of pulmonary nodules on baseline and follow-up CT examinations*. Acta Radiol 2014;55:691-698.
101. Sui X, Meinel FG, Song W, Xu X, Wang Z, Wang Y, Jin Z, Chen J, Vliegenthart R, Schoepf UJ. *Detection and size measurements of pulmonary nodules in ultra-low-dose CT with iterative reconstruction compared to low dose CT*. Eur J Radiol 2016;85:564-570.

102. Reeves AP, Chan AB, Yankelevitz DF, Henschke CI, Kressler B, Kostis WJ. *On measuring the change in size of pulmonary nodules*. IEEE Trans Med Imaging 2006;25:435-450.
103. Nair A, Baldwin DR, Field JK, Hansell DM, Devaraj A. *Measurement methods and algorithms for the management of solid nodules*. J Thorac Imaging 2012;27:230-239.
104. Li B, Avinash G, Claus B, Metz S. *3-D view weighted cone-beam filtered backprojection reconstruction for digital tomosynthesis*. Proc. of SPIE 2007; 6510:65104X-1-65104X-8.
105. Svalkvist A. *Development of methods for evaluation and optimization of chest tomosynthesis*. University of Gothenburg, Gothenburg, Sweden 2011; Doctoral thesis.
106. Ullman G, Dance DR, Sandborg M, Carlsson GA, Svalkvist A, Båth M. *A Monte Carlo-based model for simulation of digital chest tomosynthesis*. Radiat Prot Dosimetry 2010;139:159-163.
107. Börjesson S, Håkansson M, Båth M, Kheddache S, Svensson S, Tingberg A, Grahn A, Ruschin M, Hemdal B, Mattsson S, Månsson LG. *A software tool for increased efficiency in observer performance studies in radiology*. Radiat Prot Dosimetry 2005;114:45-52.
108. Håkansson M, Svensson S, Zachrisson S, Svalkvist A, Båth M, Månsson LG. *ViewDEX: an efficient and easy-to-use software for observer performance studies*. Radiat Prot Dosimetry 2010;139:42-51.
109. Svalkvist A, Svensson S, Håkansson M, Båth M, Månsson LG. *ViewDEX: a status report.* Radiat Prot Dosimetry 2016;169:38-45.
110. Dunn OJ. *Multiple comparisons among means*. 1961;56:52-64.
111. Kendall MG. *A new measure of rank correlation*. Biometrika 1938;30:81-93.
112. Båth M, Håkansson M, Hansson J, Månsson LG. *A conceptual optimisation strategy for radiography in a digital environment*. Radiat Prot Dosimetry 2005;114:230-235.
113. Jadidi M, Sundin A, Aspelin P, Båth M, Nyren S. *Evaluation of a new system for chest tomosynthesis: aspects of image quality of different protocols determined using an anthropomorphic phantom*. Br J Radiol 2015;88:20150057.
114. Abdurahman S, Jerebko A, Mertelmeier T, Lasser T, Navab N, *Out-of-plane artifact reduction in tomosynthesis based on regression modeling and outlier detection* in *Breast Imaging*, A.D.A. Maidment, P.R. Bakic, and S. Gavenonis, Editors. 2012, Springer: Berlin Heidelberg. p. 729-736.
115. Wu T, Moore RH, Kopans DB. *Voting strategy for artifact reduction in digital breast tomosynthesis*. Med Phys 2006;33:2461-2471.
116. Loog M, van Ginneken B, Viergever MA. *Segmenting the posterior ribs in chest radiographs by iterated contextual pixel classification*. Proc. of SPIE 2003; 5032:609-618.
117. Godfrey DJ, McAdams HP, Dobbins JT, 3rd. *Optimization of the matrix inversion tomosynthesis (MITS) impulse response and*

modulation transfer function characteristics for chest imaging. Med Phys 2006;33:655-667.
118. Warp RJ, Godfrey DJ, Dobbins III JT. *Application of matrix inverse tomosynthesis*. Proc. of SPIE 2000; 3977:376-383.
119. Juluru K, Al Khori N, He S, Kuceyeski A, Eng J. *A mathematical simulation to assess variability in lung nodule size measurement associated with nodule-slice position*. J Digit Imaging 2015;28:373-379.
120. Ko JP, Berman EJ, Kaur M, Babb JS, Bomsztyk E, Greenberg AK, Naidich DP, Rusinek H. *Pulmonary Nodules: growth rate assessment in patients by using serial CT and three-dimensional volumetry*. Radiology 2012;262:662-671.
121. Revel MP, Merlin A, Peyrard S, Triki R, Couchon S, Chatellier G, Frija G. *Software volumetric evaluation of doubling times for differentiating benign versus malignant pulmonary nodules*. AJR Am J Roentgenol 2006;187:135-142.
122. Arvidsson J, Söderman C, Allansdotter Johnsson Å, Bernhardt P, Starck G, Kahl F, Båth M. *Image fusion of reconstructed digital tomosynthesis volumes from a frontal and a lateral acquisition*. Radiat Prot Dosimetry 2016;169:410-415.
123. den Harder AM, Willemink MJ, van Hamersvelt RW, Vonken EP, Schilham AM, Lammers JW, Luijk B, Budde RP, Leiner T, de Jong PA. *Pulmonary Nodule Volumetry at Different Low Computed Tomography Radiation Dose Levels With Hybrid and Model-Based Iterative Reconstruction: A Within Patient Analysis*. J Comput Assist Tomogr 2016;40:578-583.
124. Månsson LG, Båth M, Mattsson S. *Priorities in optimisation of medical X-ray imaging-a contribution to the debate*. Radiat Prot Dosimetry 2005;114:298-302.
125. Zhong Y, Lai CJ, Wang T, Shaw CC. *A dual-view digital tomosynthesis imaging technique for improved chest imaging*. Med Phys 2015;42:5238-5251.